APPENDIX III : DESCRIPTION OF THE SUBROUTINES

Contents

Description of the differents subroutines used to compute the geometrical conditions:

Description of the subroutines used to compute the different atmospheric functions:

Description of the subroutines used for BRDF ground

Description of the subroutines used to update atmospheric profile (airplane, elevated target):

Description of the different subroutines used to read the data:

Miscellaneous

DESCRIPTION OF THE SUBROUTINES USED

TO COMPUTE THE GEOMETRICAL CONDITIONS

SUBROUTINE POSGE

Function: Same as POSMTO but for GOES East satellite. We use exactly the same scheme, only we add the longitude of the subsatellite point, namely 75W, at the retrieval longitude. Let us also recall that the dimension of the frame is 17331 × 12997 and the altitude of the satellite is 35729 km.

SUBROUTINE POSGW

Function: Same as POSMTO but for GOES West satellite. We use exactly the same scheme but we add the longitude of the subsatellite point, namely 135W, at the retrieval longitude. Let us recall that the dimension of the frame is 17331 × 12997 and the altitude of the satellite is 35769 km.

SUBROUTINE POSLAN

Function: To compute the geometrical conditions for the LANDSAT satellite. As the dimensions of the frame are 180 ×180 km, the maximum observation angle is 5.5°, so we put θ_V = 0. The incident conditions are taken from the latitude and the longitude of the centre of the scene.

Reference:

NASA, 1981, GSFC specification for the Thematic Mapper Subsystem and associated test equipment. Revision C., GSFC 400-8-D.210C, NASA/GSFC, Greenbelt, Maryland, U.S.A..

SUBROUTINE POSMTO

Function: To compute the geometrical conditions from the knowledge of the line number and the pixel in the line (in Meteosat Frame 2500*5000). Firstly, we compute the latitude and the longitude of the pixel, so the solar position (with the time conditions) can be computed and secondly, the observation angle.

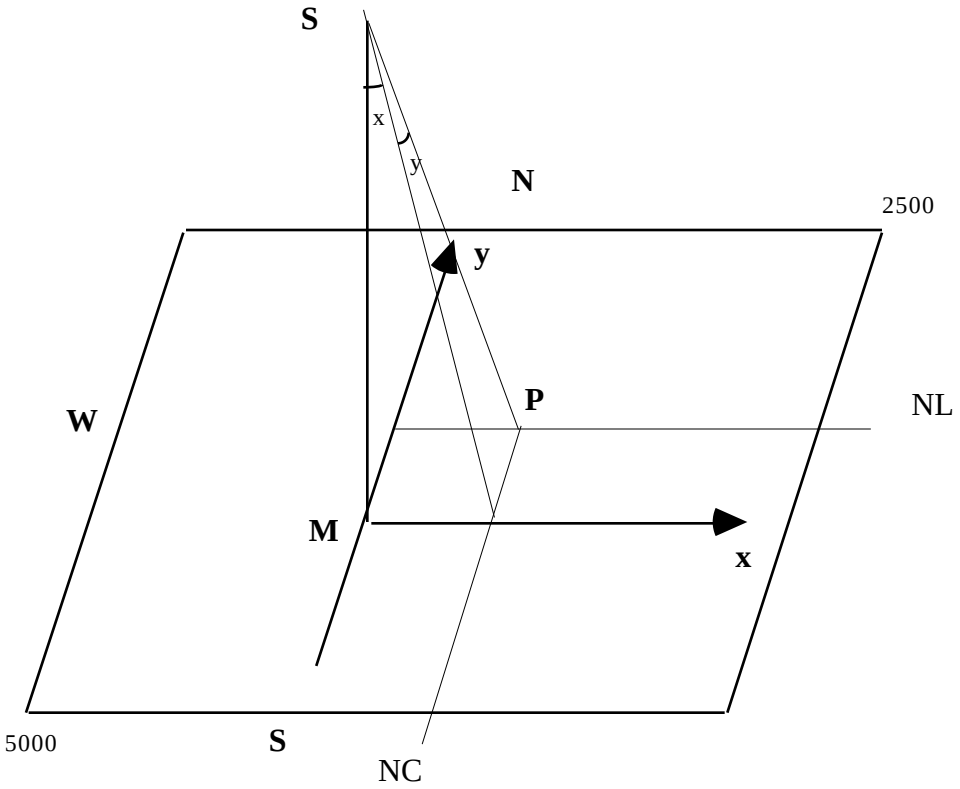

Description: Let S be the satellite, M the subsatellite point, P the observed point, and the orientation of the axes according to Fig. 1.

From N_c and N_1, we obtain the two angles X, Y with respect to x and y axes.

If we refer now to the plane containing the points S, P, M and O the center of the earth (cf. Fig. 2), we put H the altitude of the satellite and R_E the earth radius in Equatorial plane.

The observed point P corresponds to the point P' on the earth surface and we have to determine its coordinates x, y, z with respect to the axis-system centered at O.

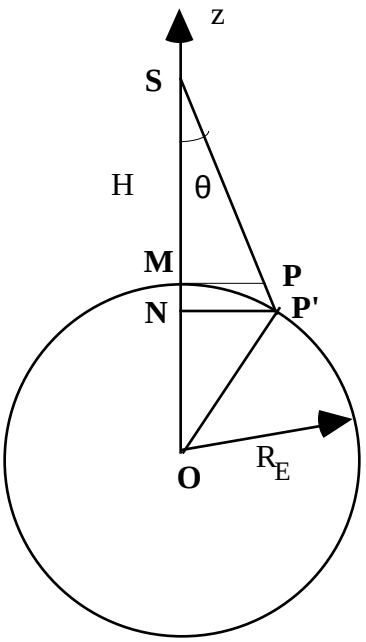

Figure 2

To obtain z, we put,

$$z = ON = (R_E+H) - SN,$$

SN is obtained from the solutions of triangles OP'S and SNP'.

• By solving OP'S, we have

$$SP'^2 - 2SP' \cos q\, OS = OP'^2 - OS^2 ,$$

so

$$SP' = \cos(\theta)(H + R_E) - \sqrt{(R_E + H)^2\left(\cos(\theta)^2 - 1\right) - R_E^2}$$

• By solving SNP' we have SN = SP' cos θ,

then $$SN = \cos(\theta)^2(H + R_E) - \cos(\theta)\sqrt{(R_E + H)^2\left(\cos(\theta)^2 - 1\right) - R_E^2}$$

Therefore :

$$z = R_E + H - \cos(\theta)^2 \left[H + R_E - R_E\sqrt{\left(\frac{R_E + H}{R_E}\right)^2 - \frac{\left(\frac{R_E + H}{R_E}\right)^2 - 1}{\cos(\theta)^2}}\right]$$

To estimate cosθ, we use the deviations X and Y. A simple trigonometrical identity shows that :

$$cos^2\theta = cos^2X.cos^2Y$$

where

$$cos^2 X = \frac{1}{1+tan^2 X}$$

and

$$cos^2 Y = \frac{1}{1+(tanY(1+\varepsilon))^2}$$

with

$$\varepsilon = \frac{R_E - R_P}{R_E} = \frac{1}{297}$$

R_E and R_P being respectively the equatorial and polar radius, slightly different because of the earth's oblateness.

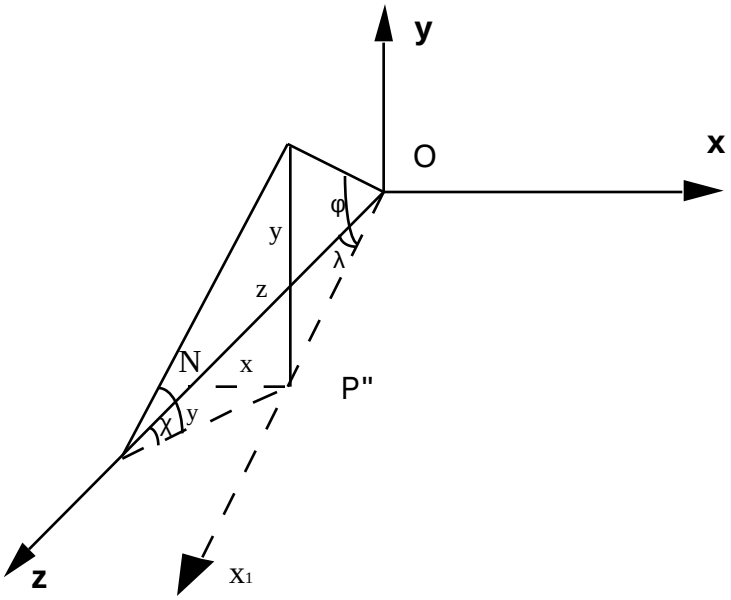

To obtain *x* and *y*, we consider the Figure 3.

$$x = -SN\ tanY$$

and

$$y = SN/cosX.tanY$$

So we have the three coordinates *x, y, z* of the point P' and infer latitude φ and longitude λ.

To compute the longitude, we use, λ = arctan (*x/z*) (+ for East, - for West).

To compute the latitude, we have to consider the geoide with semiminor axis R_p and semimajor axis R_E (Figure 4) by solving triangle P'OP". As $\varphi = atan(y/x_1)$where y is the ordinate of the point located on the ellipsoïd, so we have to compute x_1.

Figure 4

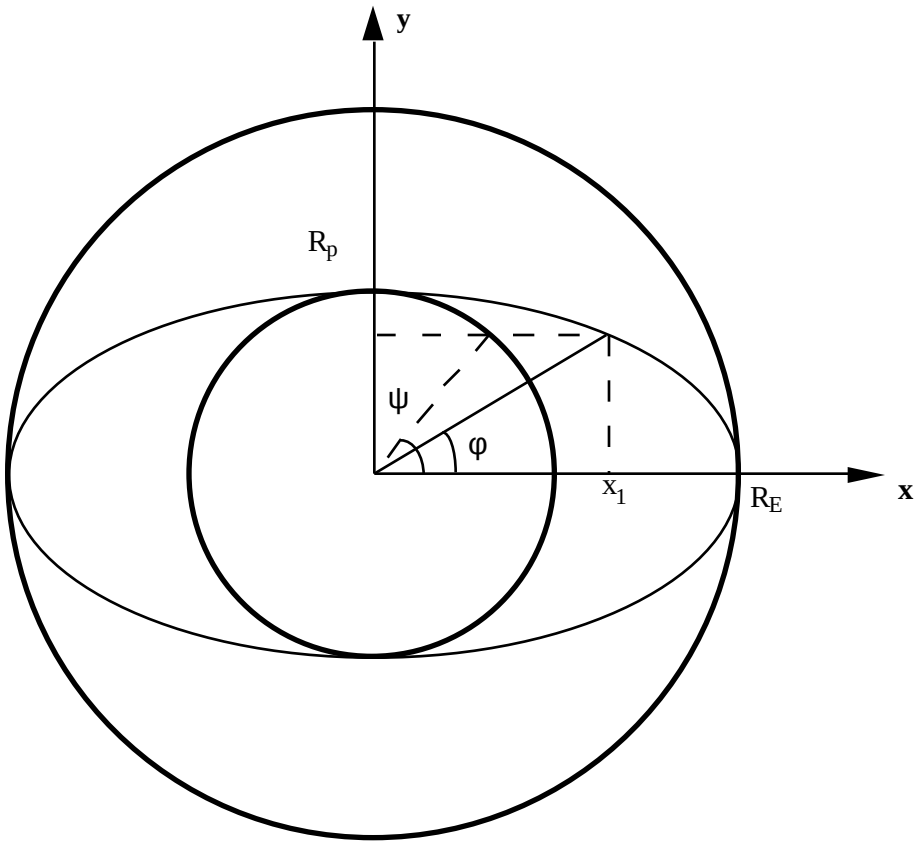

The ellipse equation is written:

$$\frac{x_1^2}{R_E^2} + \frac{y^2}{R_P^2} = 1$$

so

$$\phi = atan\left(\frac{y}{\sqrt{R_P^2 - y^2}\,(R_P/R_E)}\right),$$

$$\phi = atan(\tan\psi\,(R_P/R_E))$$

with $\Psi = asin(y/R_P)$.

To obtain observations angles (azimuthal and zenithal), we use the following simple geometrical considerations.

For the zenithal angle θ_V,

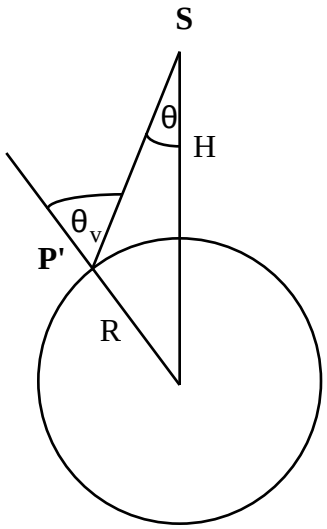

Figure 5

$$\theta_v = \text{asin}\left((1+\frac{h}{R}) \sin\theta \right)$$

where θ is so as $\cos^2 \theta = \cos^2 X \cos^2 Y$.

For the azimuthal angle φ_V, we solve the spherical triangle P'P"M

Figure 6

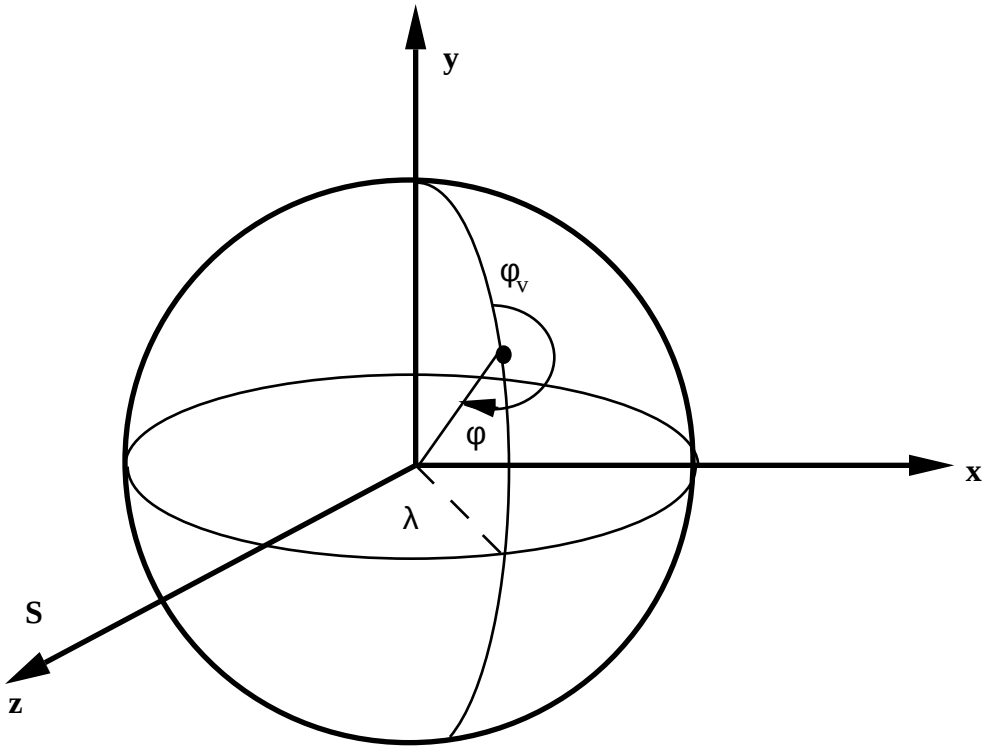

where $A = \varphi_V - \pi$,

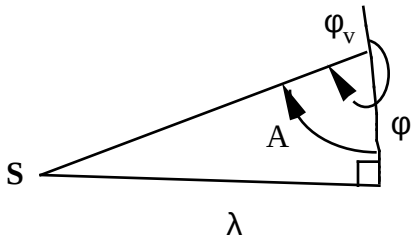

with $\tan A = \tan \lambda \, (1/\sin \varphi)$,

so $\varphi_V = \arctan[\tan \lambda (1/\sin \varphi)] + \pi$.

From the line and column numbers in a METEOSAT Frame, we can compute the latitude (φ) and the longitude (λ) of the point, and the viewing direction from the normal at the point (azimuthal φ_V and zenithal θ_V angles). Moreover, if we know the date and the hour of the acquisition, we can obtain the solar conditions (θ_s, φ_s) from the subroutine POSSOL.

Reference:

MORGAN, 1981, Introduction to the Meteosat System, *ESOC*, Darmstadt, Germany.

SUBROUTINE POSNOA

Function: To compute the geometrical conditions for the NOAA series satellites. Generally, we know the pixel number on a line, the longitude and the time of the ascendant node at the equator, and the time of the acquisition. We obtain latitude and longitude of the viewed point, the viewing angles and with the knowledge of the date, the solar geometrical conditions.

Description: The altitude of NOAA satellite is about H = 860 km, the orbit inclination 98.96°and the time of one revolution is about 101.98 mn (6119 sec.). The 1/2 angle is of maximum 55.385°and you have 2048 pixels for each line.

Figure 1

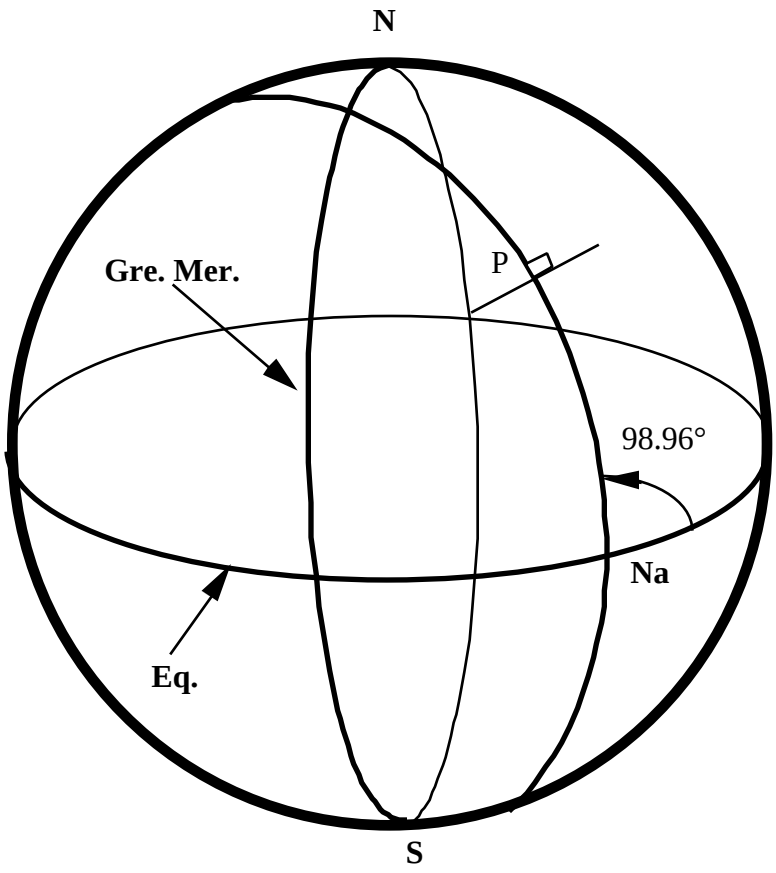

Let AN be the hour movement in rad/sec, H_N the hour at the ascendant node, λ_N its longitude and N_c the pixel number.

Figure 2

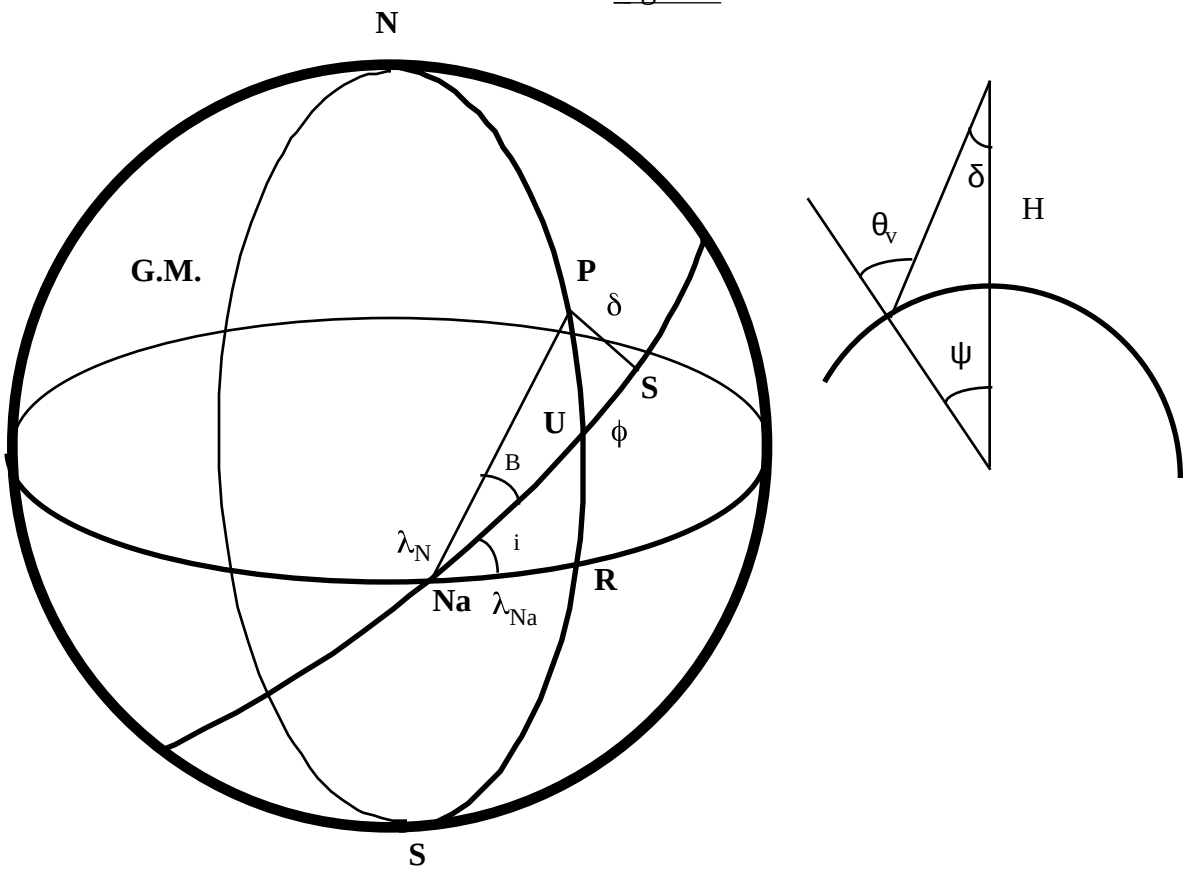

Consider Fig. 2, S is the subsatellite point, N the ascendant node and P the observed point. The scan angle δ gives an angle noted ψ at the centre of the earth.

By solving the triangle PRN, we have the latitude φ_P so as:

$$\sin \varphi_P = \sin (i+B) \sin (NP)$$

Now, in triangle PSN,

$$\sin (NP) = \sin \psi / \sin B$$

and

$$\tan (B) = \tan \psi / \sin U$$

So,

$$\sin\varphi_P = \cos i \sin\psi + \sin i \cos \psi \sin U$$

By solving PRN, we obtain the longitude λ_P with respect to λ_N ,

$$sin\,\lambda_P = sin\,NPR\,sin\,NP$$

with

$$sinNPR = \frac{cos(i + B)}{cos\phi_P} \ ,$$

so, we write

$$sin\,\lambda_P = \frac{cos(i + B)sinNP}{cos\phi_P}$$

or

$$sin\,\lambda_P = \frac{cos(i + B)sin\psi}{cos\phi_P\,sinB}$$

$$sin\,\lambda_P = \frac{-sini\,sin\psi + cos\psi\,cosi\,sinU}{cos\phi_P} \ .$$

To completly determine the longitude, we use the other relation which gives the cosine

$$cos\,\lambda_P = \frac{cos\psi\,cosU}{cos\phi_P}$$

The absolute longitude (Greenwich, Meridian reference) is given by

$$\lambda = \lambda_P + \lambda_N - \left(T - H_{Na}\right)\frac{2\pi}{86400}$$

where T is the time of the acquisition, the last term is for taking the rotation of the earth between T and H_{Na} into account. Let us recall that the movement angle U is calculated from U=AN.(T- H_{Na}).

Consider again Fig. 2 to determine the azimuthal and zenithal observation angles.
δ is so as

$$\delta = 55.385\frac{N_c - 1024}{1024} \quad \text{in deg.}$$

the zenithal viewing angle θ_V is defined by

$$\theta_V = asin[(1 + \frac{H}{R})sin\delta\,]$$

The observation azimuthal angle φ_V is determinated by solving the triangle NSP,

$$\sin\phi_V = \frac{\sin(\lambda_S - \lambda_P)\cos\phi_s}{\sin\psi}$$

and

$$\cos\phi_V = \frac{\sin\phi_S - \sin\phi_P \cos\psi}{\cos\phi_P \sin\psi}$$

where φ_S and λ_S are the latitude and the longitude of the subsatellite point P.

Reference:

The characteristics of the orbit have been taken from, NOAA POLAR ORBITER DATA USERS GUIDE, 1985, U.S. Department of Commerce, NOAA: National Environment Satellite, National Climatic Data Center, Satellite Data Service Division, World Weather Building, Room 100, Washington DC 20233, U.S.A..

SUBROUTINE POSSOL

Function: To compute the solar azimuthal and zenithal angles (in degrees) for a point over the globe defined by its longitude and its latitude (in dec. degrees) for a day of the year (fixed by number of the month and number of the day in the month) at any Greenwich Meridian Time (GMT dec. hour).

Figure 1

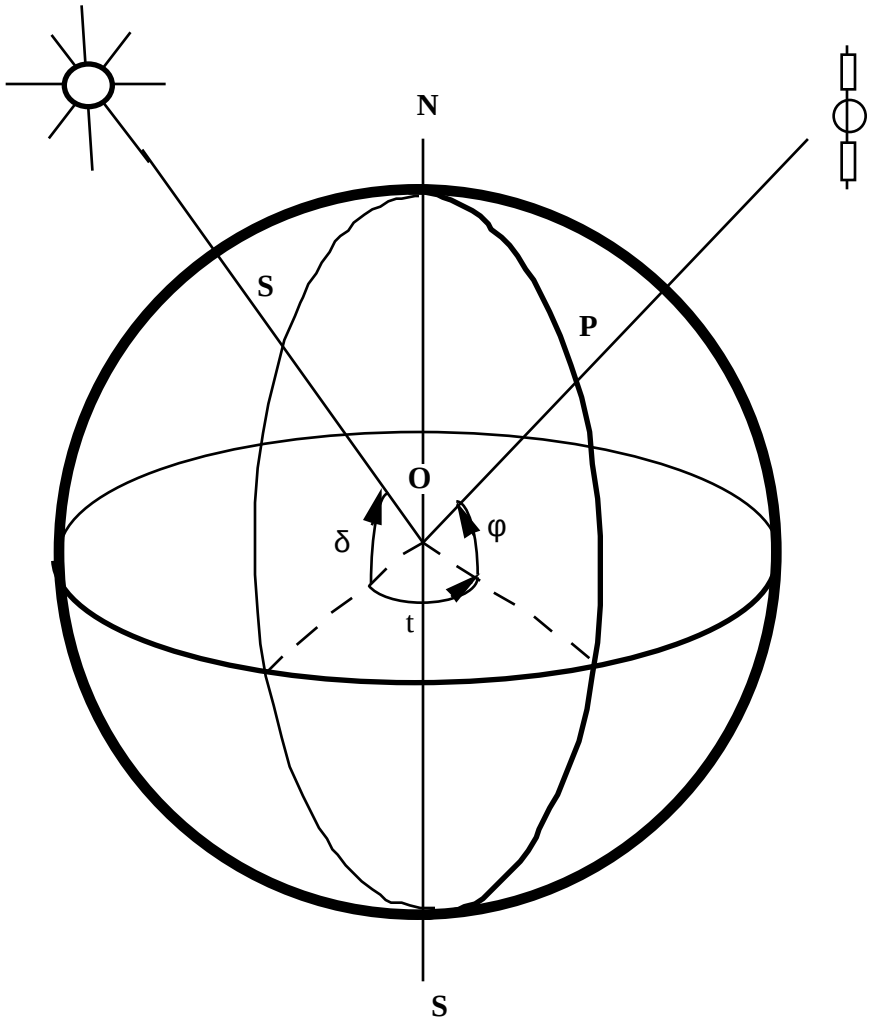

Description: Let P be the point determined by the latitude φ and δ the declination of the sun at this period of the year, the hour angle is noted t. So the incident angle θ_S can be determined by spherical trigonometry expression

$$\cos\theta_S = \cos(\frac{\pi}{2} - \delta)\cos(\frac{\pi}{2} - \varphi) + \sin(\frac{\pi}{2} - \delta)\sin(\frac{\pi}{2} - \varphi)\cos t$$

or

$$\cos\theta_v = \sin\delta\sin\varphi + \cos\delta\cos\varphi\cos t$$

The solar declination depends upon the day of the year. We used the decomposition in Fourier series of the declination based on astronomical data with the expression:

$$\delta = \beta_1 - \beta_2\cos(A) + \beta_3\sin(A) - \beta_4\cos(2A) + \beta_5\sin(2A) - \beta_6\cos(3A) + \beta_7\sin(3A)$$

where $A = \frac{2\pi J}{365}$ and J is the julian day

β_1=.006918, β_2=.399912, β_3=.070257,
β_4=.006758, β_5=.000907, β_6=.002697, β_7=.001480

The hour angle is computed from the following considerations. From the GMT time, we compute the mean solar time (or local time) for the longitude λ

$$MST = GMT + \frac{\lambda}{15}\ (dec.hour)\ .$$

The length of the day changes within the year (differences between +30 s and - 20 s), so we have to correct the local time to obtain the true solar time (TST).

$$TST = MST + ET$$

where the equation of time ET is given by:

$$ET = \frac{(\alpha_1 + \alpha_2\cos(B) - \alpha_3\sin(B) - \alpha_4\cos(2B) - \alpha_5\sin(2B))12}{\pi} \qquad (dec.hour)$$

with

$$B = \frac{2\pi J}{365}\ ,\ \alpha_1 = .000075,\ \alpha_2 = .001868,\ \alpha_3 = .032077,\ \alpha_4 = .014615,\ \alpha_5 = .040849$$

We obtain the hour angle t

$$t = 15 \frac{\pi}{180} (TST-12) \text{ (radians)}$$

and can compute θ_S.

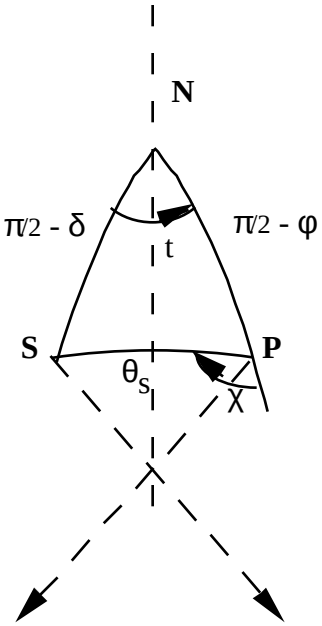

Figure 2

To determine the azimuthal angle φ_S, we solve the spherical triangle NSP:

$$\frac{\sin\chi}{\sin(\frac{\pi}{2}-\delta)} = \frac{\sin t}{\sin\theta_S}$$

where χ is the solar azimuthal angle measured from the south through the west.
Or

$$\sin\chi = \cos\delta \frac{\sin t}{\sin\theta_S} .$$

To determine the sign of χ we use the cosine

$$\cos\chi = \frac{\cos\varphi\sin\delta + \cos\delta\cos t}{\sin\theta_S}$$

so χ is completly defined.

To define the solar azimuthal angle φ_S with respect to North, we write,

$$\varphi_S = \pi + \text{asin}\ \chi.$$

References:

Ch. PERRIN DE BRICHAMBAUT, Rayonnement Solaire et Echanges Radiatifs Naturels, *Monographies de Météorologie*, Gauthier-Villars, Paris, France, 1963.

N. ROBINSON, Solar Radiation, *Elsevier Publishing Company*, New-York, N.Y., 10017, 1966.

Figure 3: Simulation of solar angles for the 1rst May, at different Latitudes, versus Universal Time.

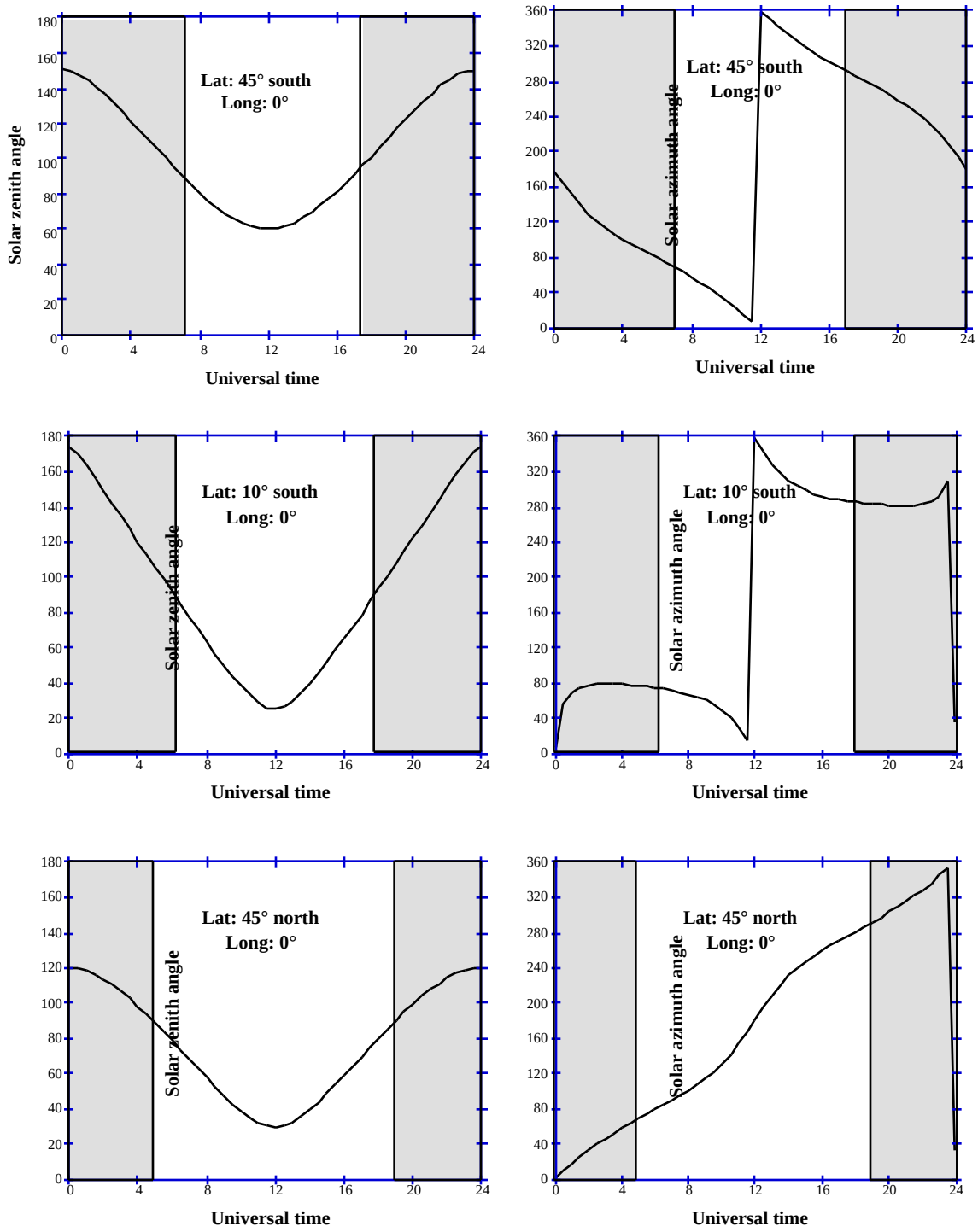

SUBROUTINE POSSPO

Function: To compute the geometrical conditions for the SPOT satellite. As the dimensions of the frame are 60 × 60 km with an observation angle of maximum 2.06°, we have considered that:

- the zenithal observation angle is nul, so the azimuthal angle is not defined,
- the incident conditions are the same that those computed for the center of the frame.

Note: We have not considered the off nadir viewing.

Reference:

M. CHEVREL , M. COURTOIS, G. WEILL (1981). The SPOT Satellite Remote Sensing Mission, *Photogrammetric Engineering and Remote Sensing*, 47, 1163-1171.

DESCRIPTION OF THE SUBROUTINES USED

TO COMPUTE THE ATMOSPHERIC CONDITIONS

SUBROUTINE ABSTRA

Function: To compute the gaseous transmittance between 0.25 and 4 μm for downward, upward and total paths. We consider the six gases (O_2, CO_2, H_2O, O_3, N_2O and CH_4) separately. The total transmission is put equal to the simple product of each ones. The spectral resolution is equal to 10 cm^{-1}.

Description: We have used two random exponential band models (*Goody* for H_2O and *Malkmus* for O_2, CO_2, O_3, N_2O and CH_4) to compute the gaseous transmissions. If we consider an homogeneous path, the transmission function is written,

for H2O

$$t_{\Delta\nu}^{G} = exp\left[- \frac{N_0 \; k \, m}{\Delta\nu} \left(1 + \frac{k \, m}{\Pi \; \alpha_0} \right)^{-\frac{1}{2}} \right] \tag{01}$$

for the other gases

$$t_{\Delta\nu}^{M} = exp\left[- \frac{2\Pi \; \alpha_0 \; N_0}{\Delta\nu} \left(\left(1 + \frac{k \, m}{\Pi \; \alpha_0} \right)^{\frac{1}{2}} - 1 \right) \right] \tag{02}$$

where m is the absorber amount, N_0 the total line number in the frequency interval $\Delta\nu$, k the average intensity and α_0 the average *Lorentz* half width, obtained from intensity S_j and half width α_j of the j^{th} spectral line by

$$k = \frac{\sum_{j=1}^{N_0} S_j}{N_0} \tag{03}$$

$$\frac{k}{\Pi\alpha} = \frac{1}{4}\left[\frac{\sum_{j=1}^{N_0} S_j}{\sum_{j=1}^{N_0}\left(S_j\,\alpha_j\right)^{1/2}}\right]^2 \qquad (04)$$

The spectral resolution of 10 cm^{-1} is sufficient and contains enough spectral lines to use a random band model transmission function.

From a general point of view, the width of a spectral line corresponds to the convolution product of the two shapes, *Lorentz* and *Doppler* and is therefore called a *Voigt* line. For an atmospheric gas (O_2, CO_2, H_2O, O_3, N_2O and CH_4) the altitude where the *Lorentz* width and *Doppler* width are equivalent, is about 30 km. So, according to the vertical distribution, only O_3 requires a more complex treatment to take into account a *Voigt* profile. The O_3 visible transmission is computed by an other method detailed in the next part and the absorption in the solar infrared (3.3 μm) is very small (cf. Fig. I-2 of the chapter 1, §1). Therefore, we have used the same formalism for all gases. The approximation contributes no consequential error.

Equations (1) and (2) are valid for a homogeneous path, where pressure and temperature are assumed to be constant. To take into account the variations of temperature and pressure along the atmospheric path, we use the *Curtis-Godson* approximation which associates an amount $\overline{m}$ weighted by temperature (thereby related to the line intensity), and a amount $\overline{m\varphi}$ weighted by pressure and temperature (thereby related to the intensity and half width line)

$$\overline{m}(z,z') = \int_z^{z'} \Phi(T)\, du, \qquad (05)$$

$$\overline{m\varphi}(z,z') = \int_z^{z'} \Psi(T)\, \varphi\, du, \qquad (06)$$

with

- $\varphi = p/p_0$ (p_0 is the standard pressure at which the measurements of spectroscopic parameters have been made)
- $du = \rho_g(dz/\mu)$ (g is the gaseous density and μ the cosine of the viewing angle).

The functions $\Phi(T)$ and $\Psi(T)$ are given by

$$\Phi(T) = \frac{\sum_{j=1}^{N_0} S_j(T)}{\sum_{j=1}^{N_0} S_j(T_r)}, \qquad (07)$$

$$\Psi(T) = \frac{\left[\sum_{j=1}^{N_0} \left[S_j(T)\,\alpha_{j0}(T)\right]^{1/2}\right]^2}{\left[\sum_{j=1}^{N_0} \left[S_j(T_r)\,\alpha_{j0}(T_r)\right]^{1/2}\right]^2}, \qquad (08)$$

with T_r the reference temperature and α_{j0} the half-width at temperature T_r and pressure p_0.

To simplify, we fit these functions with,

$$\Phi(T) = \exp\left[a(T - T_r) + b(T - T_r)^2\right], \qquad (09a)$$

$$\Psi(T) = \exp\left[a'(T - T_r) + b'(T - T_r)^2\right]. \qquad (09b)$$

The spectroscopic data are taken from the *AFGL* atmospheric absorption line parameters compilation (1991 edition). We have selected the following parameters :

- the position (in cm^{-1}),
- the integrated line strength S_j (T_r) at 296 K (in $cm^{-1}/(molecules\text{-}cm^2)$),
- the half width α_{j0} at 296 K and 1013 mb (in cm^{-1}),
- the energy of the lower transition state.

The half width at any temperature and pressure is obtained by

$$\alpha_j(p,T) = \alpha_{j0} \left(\frac{p}{p_0}\right)^{1-} \left(\frac{T_r}{T}\right)^{1/2} \qquad (10)$$

and the intensity at any temperature can be computed from the vibrational and rotational partition and the energy of the lower transition state.

Subsequently, we have taken T_r = 250 K and computed $\Phi(T)$ and $\Psi(T)$ for 3 temperatures (200, 250 and 300 K) to determine the coefficients a, a', b and b'.

Now we have a series of eight coefficients by steps of 10 cm^{-1}:

- $\frac{k}{\delta} = \frac{\sum_{j=1}^{N_0} S_j(T_r)}{\Delta\nu}$ (11)
- $\frac{\Pi\alpha_0}{\delta} = \frac{4}{\Delta\nu} \frac{\left[\sum_{j=1}^{N_0} \left[S_j(T_r)\,\alpha_{j0}(T)\right]^{1/2}\right]^2}{\sum_{j=1}^{N_0} S_j(T_r)}$ (12)
- a, a'
- b, b'
- ν_{low} the lower frequency of the interval, and $\nu_{sup} = \nu_{low} + 10$ cm^{-1}

These coefficients are read in the subroutines, WAVA1 to 6 for H_2O, OZON1 for O_3, OXYG3 to 6 for O_2 and DICA1 to 3 for CO_2 .

The weighted absorber amounts $\overline{m}$ and $\overline{m\varphi}$ are computed according to Eq. (5) and (6) and the transmission functions (which correspond to Eq. (1) and (2) for a homogeneous path) are written

$$t^G_{\Delta\nu} = \exp\left[-\frac{k\,\overline{m}}{\delta}\left(1 + \frac{k}{\Pi\,\alpha_0}\,\frac{\overline{m}^2}{\overline{m\varphi}}\right)^{-\frac{1}{2}}\right], \quad (13)$$

$$t^M_{\Delta\nu} = \exp\left[-\frac{\Pi\,\alpha_0}{\delta}\,\frac{\overline{m\varphi}}{2\overline{m}}\left(1 + \frac{4\,k}{\Pi\,\alpha_0}\,\frac{\overline{m}^2}{\overline{m\varphi}}\right)^{\frac{1}{2}} - 1\right]. \quad (14)$$

Due to the deficiency of spectroscopy data, the visible ozone transmission function is written,

$$t_{O_3}(\Delta\nu) = \exp(-A_{O_3}(\Delta\nu)\ u_{O_3}) \quad (15)$$

where u_{O_3} is the absorber amount, A_{O_3} the absorption coefficient given by *Kneizys and al*. (1980).

These coefficients are given in steps of 200 cm^{-1} between 13000 and 24200 cm^{-1} and by step of 500 cm^{-1} between 27500 - 50000 cm^{-1}.

To take into account the water vapor continuum, we use the same expression with the coefficients $A^c_{H_2O}$ are given in step of 5 cm^{-1} between 2350 and 2420 cm^{-1}.

A comparison between MODTRAN2 and our results (6S) is shown in the following figures (1-3). The difference observed at roughly 3.1µm is due to the fact that we have not taken into account the N_2O continuum. This spectral range is already contaminated by water vapor and is not an atmospheric window. Therefore, the 3.1µm region is not used in remote sensing and its emission in 6S generally unimportant.

References:

A.R. CURTIS, The computation of radiative heating rates in the atmosphere, *Proc. Roy. Soc. London*, A236, p. 156-159, 1956.

R.G. ELLINGSON, J.C. GILLE, An infrared radiative transfer model. part 1: Model description and comparison of observations with calculations, *J. Atmos. Sci*. 35, p. 523-545, 1978.

R.M. GOODY, Atmospheric Radiation 1, Theoretical Basis, *Oxford University Press*, 436 pp, 1964.

F.X. KNEIZYS, E.P. SHETTLE, W.O. GALLERY, J.H. CHETWYND Jr.L.W. ABREU, J.E.A. SELBY, R.W. FENN, R.A. Mc CLATCHEY, Atmospheric Transmittance/Radiance: Computer Code LOWTRAN 5, AFGL-TR-80-0067, *Air Force Geophysics Laboratory, Bedford, Mass*. 1980.

W. MALKMUS, Random Lorentz Band Model with Exponential- Tailed S^{-1} Line-intensity Distribution Function, *J. Opt. Soc. Am*. 57, 3, p. 323-329, 1967.

J.J. MORCRETTE, Sur la Paramétrisation du Rayonnement dans les Modèles de la Circulation Génèrale Atmosphérique, *Thèse d'Etat no 630, Université de Lille*.

D.C. ROBERTSON, L.S. BERNSTEIN, R. HAIMES, J. WUNDERLICH, L. VEGA, 5 $cm^{-1.}$ Band Model Option to Lowtran 5, *Applied Optics,* 20, p. 3218-3226, 1981.

C.D. RODGERS, C.O. WALSHAW, The Computation of Infrared Cooling Rates in Planetary Atmospheres, *Quart. J. Roy. Meteor. Soc*., 92, p. 67-92, 1966.

L.S. ROTHMAN, R.R. GAMACHE, A. BARBE, A. GOLDMAN, J.R. GILLIS, L.R. BROWN, R.A. TOTH, J.M. FLAUD, C. CAMY-PEYRET, AFGL Atmospheric Absorption Line Parameters Compilation: 1982 Edition, *Applied. Optics*, 22, p. 2247-2256, 1983.

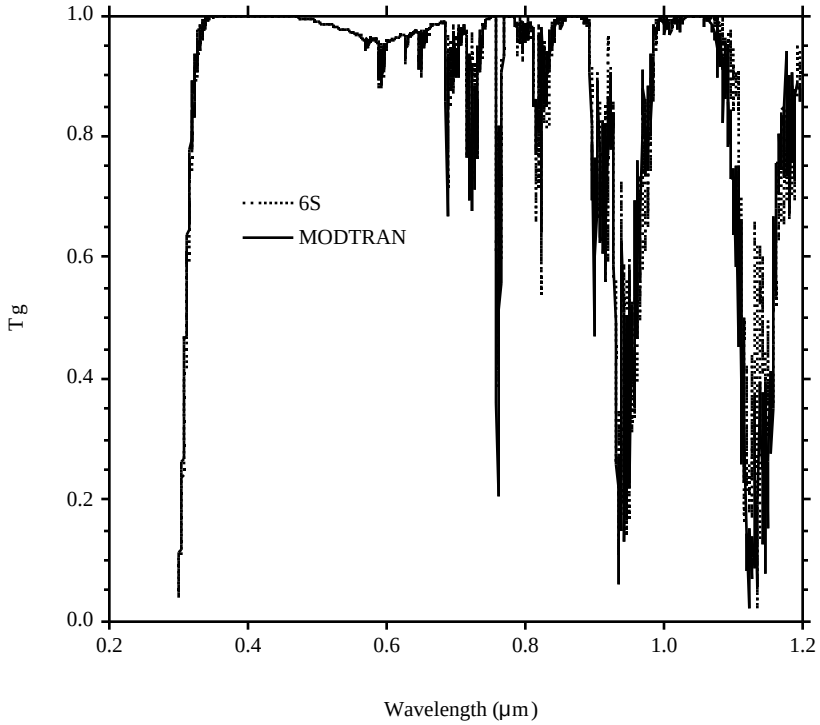

Figure 1: Gaseous transmission between 0.25 and 1.2µm (mid. lat. summer atmosphere)

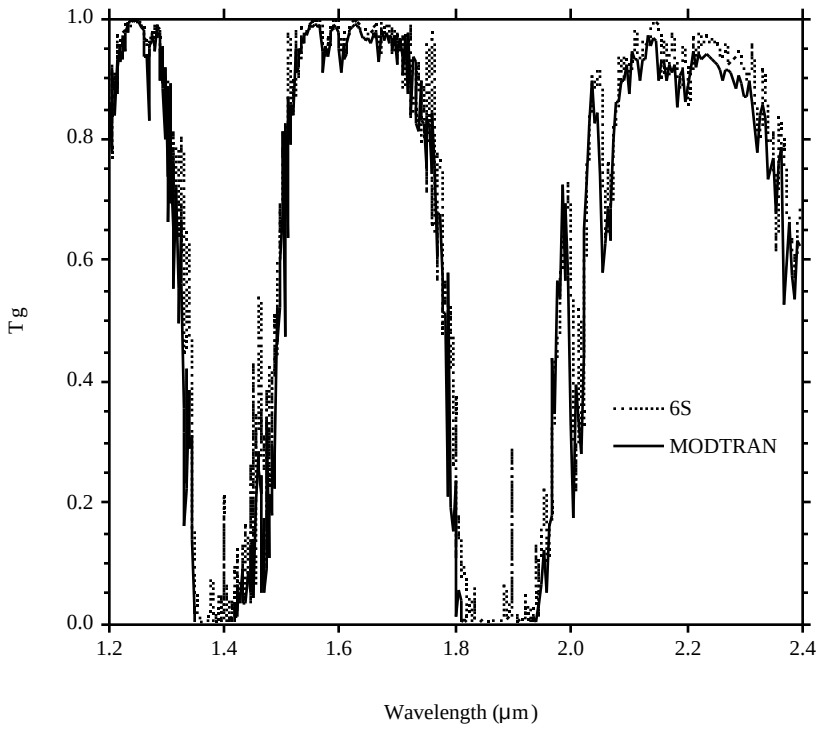

Figure 2: Gaseous transmission between 1.20µm and 2.40µm (mid. lat. summer atmosphere).

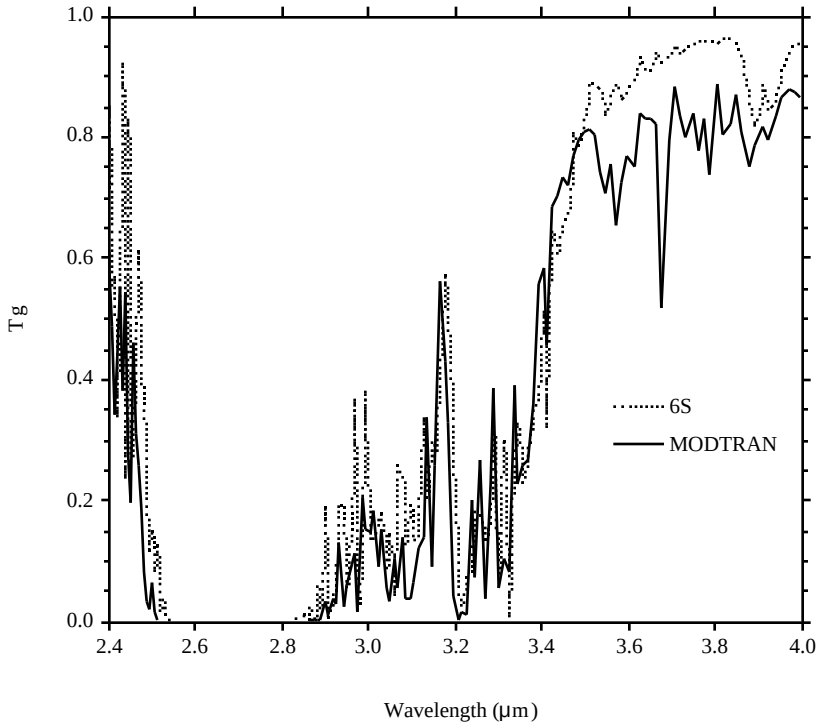

Figure 3: Gaseous transmission between 2.40µm and 4.00µm (mid. lat. summer atmosphere).

SUBROUTINE AEROSO

Function: To compute the optical scattering parameters (extinction and scattering coefficients, single scattering albedo, phase function, assymetry factor) at the ten discrete wavelengths for the selected model (or created model) from:

(1) the characteristics of the basic components of the *International Radiation Commission.* (1983).

- dust-like component (D.L., SUBROUTINE DUST)
- oceanic component (O.C., SUBROUTINE OCEA)
- water-soluble component (W.S., SUBROUTINE WATE)
- soot component (S.O., SUBROUTINE SOOT)

(2) pre-computed caracteristics,

now available are the desertic aerosol model corresponding to background conditions, as described in *Shettle*(1984), a stratospheric aerosol model as measured Mona Loa (Hawaii) during El Chichon eruption and as described by *King et al.* (1984), and a biomass burning aerosol model as deduced from measurements taken by sunphotometers in Amazonia. (SUBROUTINES BDM, STM and BBM)

(3) computed using the MIE theory with inputs (size distribution, refractive indexes...) given by the user (see SUBROUTINES MIE and EXSCPHASE).

These models don't correspond to a mixture of the four basic components.

Description: From the MIE theory (see SUBROUTINE MIE), we have computed the phase function $P(\Theta)$, the extinction and scattering coefficients, the assymetry factor g for the basic components defined by their size distributions and their refractive index. The computations were performed at 10 wavelengths and 83 phase angles (80 Gauss angles, 0°, 90°, 180°)

Note: We compute the resultant phase function for the scattering angle by linear interpolation in the table of 83 values.

From the four basic components, three tropospheric aerosols types models have been selected by mixing with the following volume percentages. By mixing, we suppose an idea of "external mixing" in the model construction, so the resultant values are obtained by a weighted average using the volume percentages C_j given by:

	D.L.	W.S.	O.C.	S.O.
Continental	0.70	0.29		0.01
Maritime		0.05	0.95	
Urban	0.17	0.61		0.22

For each component, we know the volume concentration V_j and the particle number concentration N_j (particle/cm^3):

	D.L.	W.S.	O.C.	S.O.
V_j μ^3/cm^3	113.98352	$113.98352\ 10^{-06}$	5.14441	$59.777553\ 10^{-06}$
$N_{j\ part/}cm^3$	54.73400	$1.86850\ 10^{+06}$	276.0500010	$1.805820\ 10^{+06}$

where

$$V_j = \frac{4\Pi}{3}\int_0^{+\infty} r^3 \frac{dN_j(r)}{dr}\,dr$$

and N_j is computed so as to normalize the extinction coefficient at 550 nm .

If C_j is the aerosol fraction by volume of the component j, we have $C_j = v_j / v$ with $v_j = n_j V_j$ where n_j is the number of particles in the mixing so

$$n = \sum_j n_j = v \sum_j \frac{C_j}{V_j}$$

then we can obtain the percentage density of particles

$$\frac{n_j}{n} = \frac{\frac{C_j}{V_j}}{\sum_j \frac{C_j}{V_j}}$$

so for example n_j/n for the 3 selected models:

	D.L.	W.S.	O.C.	S.O.
Continental	$2.26490\ 10^{-06}$	0.938299		0.0616987
Maritime		0.999579	$4.20823\ 10^{-04}$	
Urban	$1.65125\ 10^{-07}$	0.592507		0.407492

To obtain the extinction coefficient of the resultant model, we compute

$$K^{ext}(\lambda) = \sum_j \frac{n_j}{n} K_j^{ext}(\lambda)$$

and we normalize also this coefficient at 550 nm. So we have to compute the equivalent number N of particles by :

$$N = \frac{1}{\sum_j \frac{n_j}{n} K_j^{ext}(550)}$$

Since $K_j^{ext}(550) = 1/N_j$, we obtain

$$\frac{1}{N} = \sum_j \frac{n_j}{n} \frac{1}{N_j}$$

The other optical parameters are computed by the same way:

• scattering coefficient :

$$K^{sca}(\lambda) = N \sum_j \frac{n_j}{n} K_j^{sca}(\lambda)$$

• assymetry factor :

$$g(\lambda) = \frac{N}{K^{sca}(\lambda)} \sum_j \frac{n_j}{n} g_j(\lambda) K_j^{sca}(\lambda)$$

• phase function :

$$P_\lambda(\Theta) = \frac{N}{K^{sca}(\lambda)} \sum_j \frac{n_j}{n} P_\lambda^j(\Theta) K_j^{sca}(\lambda)$$

• the single scattering albedo is directly obtained by the ratio

$$\omega_0(\lambda) = \frac{K^{sca}(\lambda)}{K^{ext}(\lambda)}$$

Notes:

- The data for extinction or scattering coefficients are in km^{-1}

- The following figures give us an order of magnitude of these terms for the 3 selected aerosol models plus the desert aerosol model.

Reference:

World Meteorological Organization (CAS)/Radiation Commission of IAMAP Meeting of experts on aerosols and their climatic effects, WCP 55, Williamsburg, Virginia, U.S.A., 28-30 March 1983.

E. P. SHETTLE, Optical and radiative properties of a desert aerosol model. *Symposium of Radiation in the atmosphere*, 1 Deepak publishing), pp. 74-77, 1984.

M. KING, HARSHVARDHAN, and ARKING, A, A model of the Radiative Properties of the El Chichon Stratospheric Aerosol Layer, *J. Appl. Meteor.*, 23, (7), pp. 1121-1137, 1984.

Figure 1: Spectral dependence of the extinction coefficient for various aerosol models.

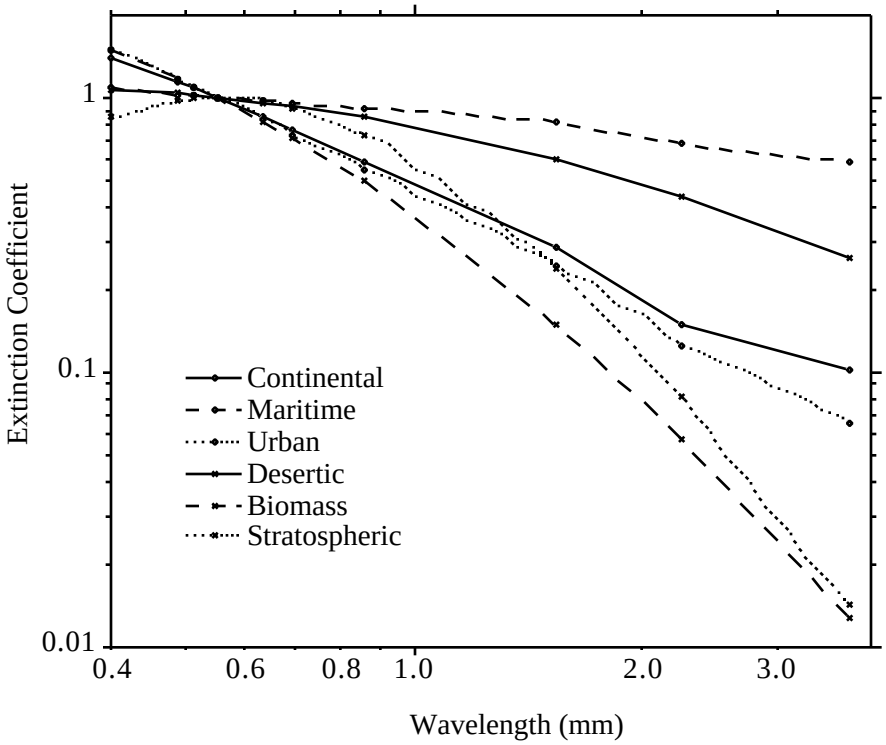

Figure 2: Spectral dependence of the single scattering albedo for various aerosol models.

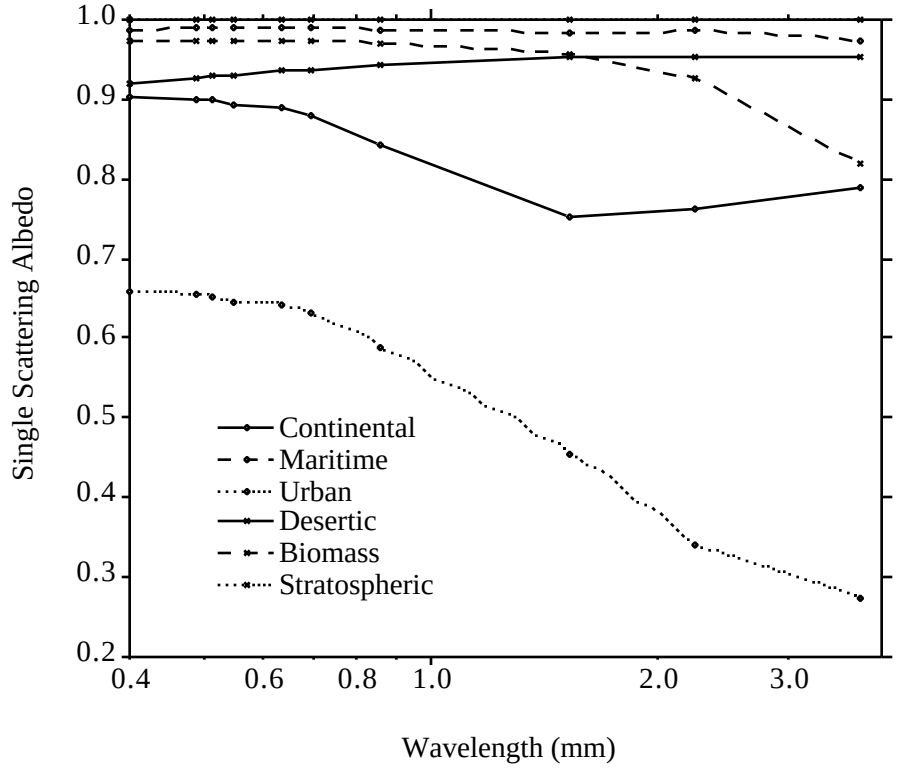

Figure 3: Spectral dependence of the assymetry parameter for various aerosol models.

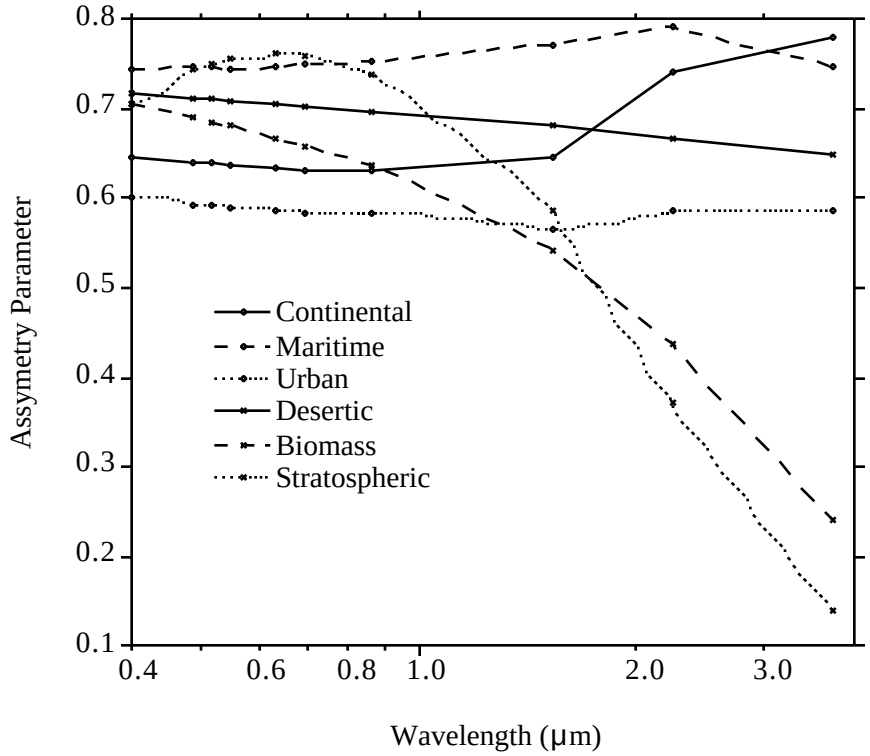

Figure 4: Phase function at 0.550μm versus scattering angle for various aerosol models.

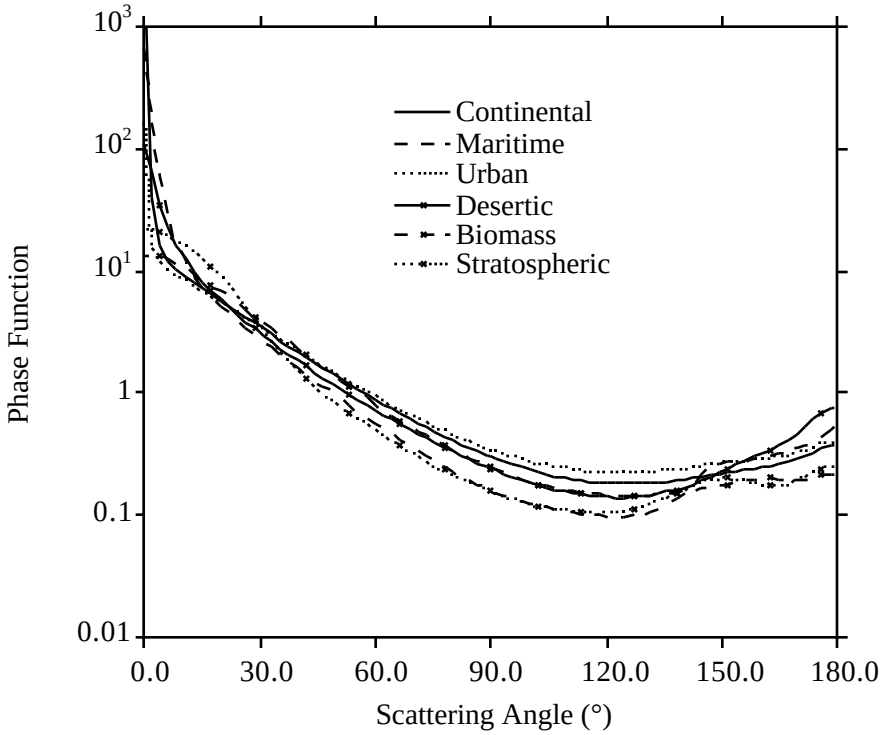

SUBROUTINE ATMREF

Function: To compute the atmospheric reflectance for the molecular and aerosol atmospheres and the mixed atmosphere. In 6S instead of an approximation as in 5S, we use the scalar Successive Order of Scattering method (subroutine OS.f). The polarization terms of aerosol or rayleigh phase are not accounted for in the computation of the aerosol reflectance and the mixed Rayleigh-aerosol reflectance. The polarization is addressed in computing the Rayleigh reflectance (Subroutine CHAND.f) by semi-empirical fitting of the vectorized Successive Orders of Scattering method (*Deuzé et al*, 1989).

Description: Three reflectance terms have to be computed by ATMREF.f, the aerosol reflectance (ρ_A), the rayleigh reflectance (ρ_R) and the reflectance of the mixed Rayleigh-aerosol (ρ_{R+A}). In addition three different configurations of sensor position are possible, ground based observation, satellite sensor or airborne sensor.

In the case of ground based observations, we consider that there is no contribution of the atmosphere below the sensor and the three reflectances are simply set to zero.

For the case of satellite based observations, we can consider that all the molecules and aerosol are below the sensor. In that case, we use the subroutine OS.f to compute ρ_A and ρ_{R+A} and the subroutine CHAND.f to compute ρ_R. The subroutine OS.f is able to deal with a mixture of molecules and aerosols or with aerosol only or molecules only, by computing the signal in a set of layers for which the proportion of molecules and aerosol can be adjusted. The computation of the proportion of aerosol and molecules in each layer is optimized by the subroutine DISCRE.f to divide the entire atmosphere in equal optical depth layers, the proportion depends on the aerosol profile which is assumed to be exponential with a scale heigh of 2km.

For the case of airborne observation, the three components are computed by the OS.f subroutine. In OS.f, a special layer is set so that the top of the layer corresponds to the aircraft's altitude. When aerosol optical depth below the plane is provided by the user as encouraged, the scale height of aerosol is computed again to match the total aerosol optical depth, the aerosol optical below the plane and the plane altitude. If in that case, the scale heigh is found to be greater than 7km a warning message is issued and computation are aborted.

References:

Radiation Commission of IAMAP, Standart Procedures to compute Atmospheric Radiative Transfer in a scattering Atmosphere. Edited by J. LENOBLE, Available from Dr. S. Ruttenberg, NCAR, Boulder Colorado 80307, U.S.A., 1977.

D. TANRE, M. HERMAN, P.Y. DESCHAMPS, A. DE LEFFE, Atmospheric Modeling for Space Measurements of Ground Reflectances including bidirectional properties, *Appl. Opt*. 18, no 21, p. 3587-3594, 1979.

J. L. DEUZÉ, M. HERMAN AND R. SANTER, Fourier series expansion of the transfer equation in the atmosphere-ocean system. *Journal of Quantitative Spectroscopy and Radiative Transfer,* **41,** 6, 483-494, 1989.

SUBROUTINE CHAND

Function: To compute the atmospheric reflectance for the molecular atmosphere in case of satellite observation.

Description: In 6S, to save computer ressources but maintain a good accuracy, we used the same approach to compute the molecular scattering reflectance as it is detailled in a recent paper (*Vermote and Tanré* 1992). The molecular reflectance, as computed from 6S is plotted vs the reflectance computed from the SOS method for τ=0.35 in Fig. 1. Four values of the solar zenith angle (0°, 53°, 66° and 70°), 17 values of the viewing zenith angle (from 0° to 60° with a step of 3.3°) and 19 values of the difference of the azimuth angles (from 0° to 180° with a step of 10°), covering a large range of possible geometrical conditions, have been selected. Multiple points fall on the 45-degree line; the right-hand scale, which gives absolute differences between the two results, clearly shows that the accuracy of 0.001 is achieved for the full range of geometric conditions.

References:

E. F. VERMOTE and D. TANRE , Analytical Expressions for Radiative Properties of Planar Rayleigh Scattering Media Including Polarization Contribution. *Journal Of Quantitative Spectroscopy and Radiative Transfer*, **47,** 4, 305-314, 1992.

Figure 1: Accuracy of CHAND.f

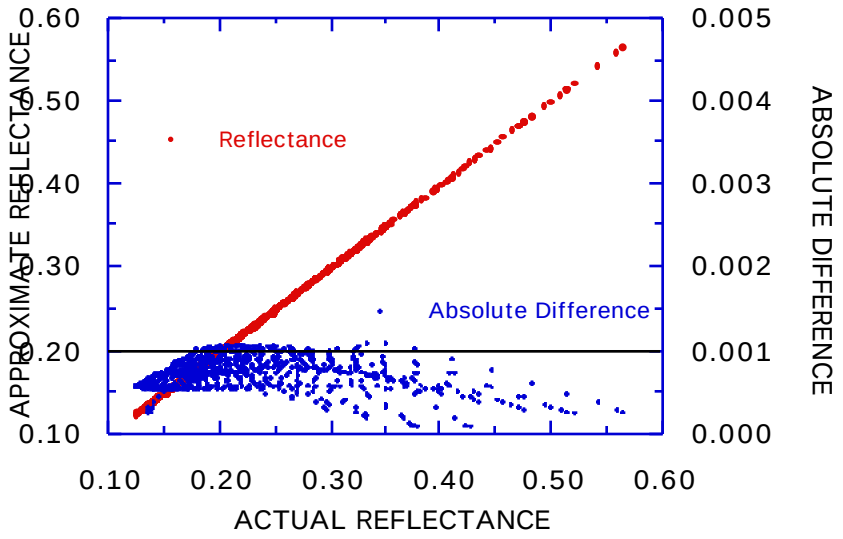

SUBROUTINE CSALBR

Function: To compute the spherical albedo of the molecular layer.

Description: We integrate the transmission function of the different incident directions to calculate the spherical albedo, s, that is:

$$s = 1 - \int_0^1 \mu\, T(\mu)\, d\mu \qquad (01)$$

Using the expression of T(μ) derived in SCATRA (Eq. 01.), it can be shown that s reduces to:

$$s = \frac{1}{4 + 3\tau}\left[3\tau - 4E_3(\tau) + 6E_4(\tau)\right] \qquad (02)$$

where $E_3(\tau)$ and $E_4(\tau)$ are exponential integrals for the argument τ. These functions are easily computable from expressions given in the reference below.

Figure 1 shows that the differences between the exact results and Eq. (02) are approximately 0.003 for τ=0.35 which results in an error of 0.0003 for a surface albedo of 0.10. In the red part of the solar spectrum for which the surface albedo may be larger, the error is still below 0.001.

References

M. ABRAMOWITZ AND I STEGUN, *Handbook of Mathematical Functions* (New-York: Dover Publications,Inc), 1970.

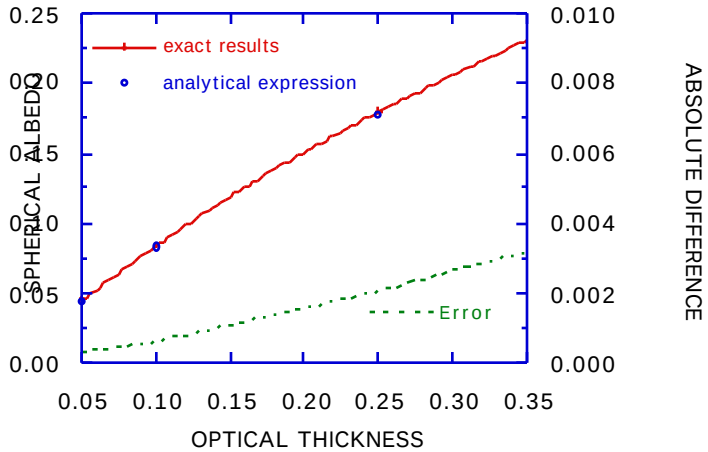

Figure 1: Accuracy of Eq. 02.

SUBROUTINE DISCOM

Function : To compute the optical properties of the atmosphere at the 10 discrete wavelengths.

Description :

The 10 wavelengths, 0.400, 0.488, 0.515, 0.550, 0.633, 0.694, 0.860, 1.536, 2.250, 3.750, have been selected because they correspond to the atmospheric windows used in remote sensing.

The computed quantities are

- molecular optical depth (subroutine ODRAYL)
- aerosol optical depth(subroutine ODA550)
- atmospheric reflectances (subroutine ATMREF)
- scattering transmittances (subroutine SCATRA)
- spherical albedos (subroutine SCATRA).

The computations have been made respectively for the 3 types of atmosphere:

- molecular
- aerosols only
- complete atmosphere with the two components.

SUBROUTINE DISCRE

Function: Decompose the atmosphere in a finite number of layers. For each layer, DISCRE provides the optical thickness, the proportion of molecules and aerosols assuming an exponential distribution for each constituants. Figure 1 illustrate the way molecules and aerosols are mixed in a realistic atmosphere. For molecules, the scale height is 8km. For aerosols it is assumed to be 2km unless otherwise specified by the user (using aircraft measurements).

Figure 1: Molecules and aerosol mixing in atmosphere.

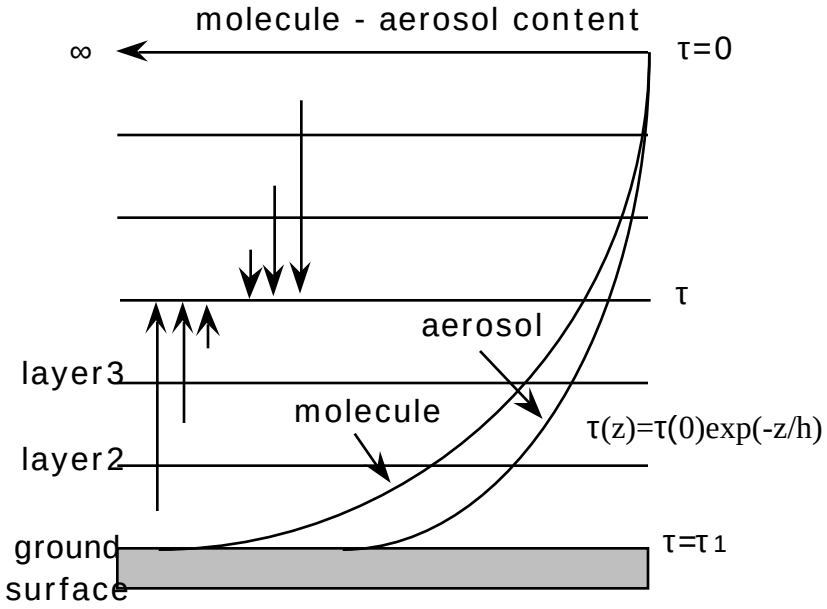

SUBROUTINE ENVIRO

Function: To compute the environment functions F(r) which allows us to account for an inhomogeneous ground.

Description: For an accurate evaluation of F(r), Monte Carlo computations are necessary to take into account

- the altitude dependence of the phase function
- the dependence of the phase function upon the aerosols type
- the scaling factors which are different for the aerosols and the molecules.

Simulations for some different vertical distributions and phase functions show that the variability of the environment function F(r) can be rather tractable.

The molecular scattering which is a major factor for the enlarged contribution of the background can be linearized and accounted for by:

$$F(r) = \frac{t_d^R(\theta_v) F^R(r) + t_d^P(\theta_v) F^P(r)}{t_d^R(\theta_v) + t_d^P(\theta_v)} \qquad (01)$$

where $t_d^R(\theta_v)$ and $t_d^P(\theta_v)$ are the diffuse fractions in the transmission functions respectively for Rayleigh and aerosols.

$F^R(r)$ and $F^P(r)$ correspond to the environment functions estimated for Rayleigh and aerosols taken into account separately, these functions are slightly dependent upon the wavelength.

We have computed these 2 functions for a mean atmosphere at the satellite level (Mc Clatchey *et al*, 1971) and we propose the following approximations:

$$F^P(r) = 1 - \left[0.448\, E^{-0.27r} + 0.552\, E^{-2.83r} \right] \qquad (02)$$

$$F^R(r) = 1 - \left[0.930\, E^{-0.08r} + 0.070\, E^{-1.10r} \right] \qquad (03)$$

where r is in km.

If the actual aerosol model (type and vertical distribution) does not differ much from the mean model, these approximations are reasonnable and we account for major part of the environment effect. Figure 1 shows the two functions $F^R(r)$ and F^Pr. We note that the horizontal scales of the environment effect are typically 1km for aerosol scattering and 10km for molecular scattering.

For the case of an airborne observation, we computed the altitude dependence of the Rayleigh and aerosol environment function. For several typical altitude we have computed $F^R(r,z)$ and $F^P(r,z)$ by the Monte Carlo method and we have derived an approximate expression (Eq. (2) and (3)). Figures 2 and 3 show, for the selected altitudes, the environment functions For a plane flying at an arbitrary altitude, we perform a linear interpolation between the closest simulated altitudes in 6S to get the environment function at the altitude of the plane.

Effect of the view zenith angle.

For 6S, we look at the dependence of these two environment functions as a function of the view zenith angle. Fig. 4a and 4b show for several values of the view zenith angle the environment function of Rayleigh and aerosol. As it can be observed on Fig. 4a-b, there is a dependence of the function F(r) on the view direction for view zenith angle larger than 30°. In order to account for this effect, we chose to fit the environment function at the desired view angle solely as a function of the environment function computed for a nadir view as it is suggested by Fig. 4a-b. The results presented on Fig. 4a-b (symbols) show that a simple polynomial function of nadir view environment function whose coefficients depend on the logarithm of the cosine of view angle is adequate. For molecules, the F function is fitted by the simple expression :

$$F_R(\theta_v) = F_R(\theta_v = 0°).\left[\ln(\cos(\theta_v).\left(1 - F_R(\theta_v = 0°)\right) + 1\right] \qquad (04)$$

for aerosol, a polynomial of a higher degree is needed, that is:

$$F_A(\theta_v) = F_A(\theta_v = 0°).\begin{bmatrix} \left[1 + a_0 \ln(\cos(\theta)) + b_0 \ln(\cos(\theta))^2\right] + \\ F_A(\theta_v = 0°).\left[a_1 \ln(\cos(\theta)) + b_1 \ln(\cos(\theta))^2\right] + \\ F_A(\theta_v = 0°)^2.\left[(-a_1 - a_0)\ln(\cos(\theta)) + (-b_1 - b_0)\ln(\cos(\theta))^2\right] \end{bmatrix} \qquad (05)$$

with a_0=1.3347, b_0=0.57757, a_1=-1.479, b_1=-1.5275

However, it has to be pointed out that if the approximations (04 and 05) enable to take into account adjacency effect for an arbitrary view angle, they implied uniformity of the background as a function of azimuth. As contributions of the adjacent pixels for a large view angle don't comply to the symmetry in azimuth, the 6S results, in case of large view angles, have to be interpreted more like a sensitivity test to the problem of adjacency effect rather than an actual way to perform adjacency effect correction .

Reference:

D. TANRE, M. HERMAN and P.Y. DESCHAMPS, Influence of the background contribution upon space measurements of ground reflectance, *Appl. Opt.*, 20, p. 3676-3684, 1981.

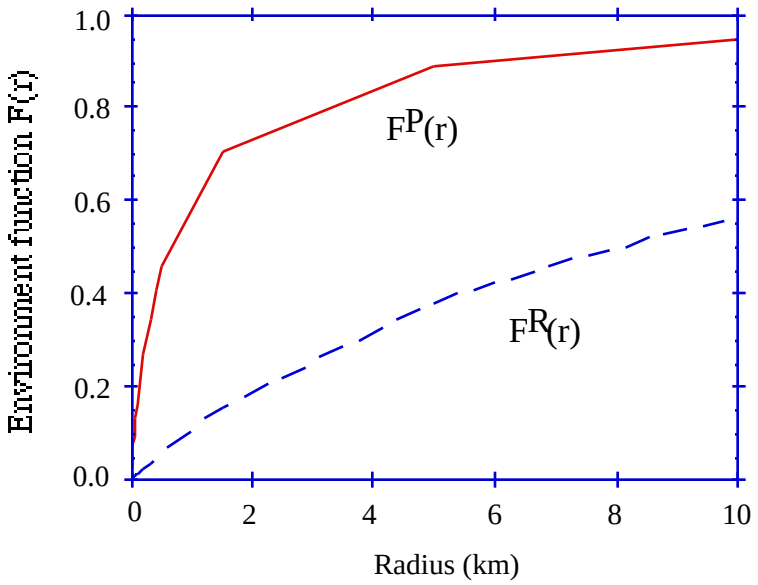

Figure 1: Environment function at satellite level for Rayleigh and Particules.

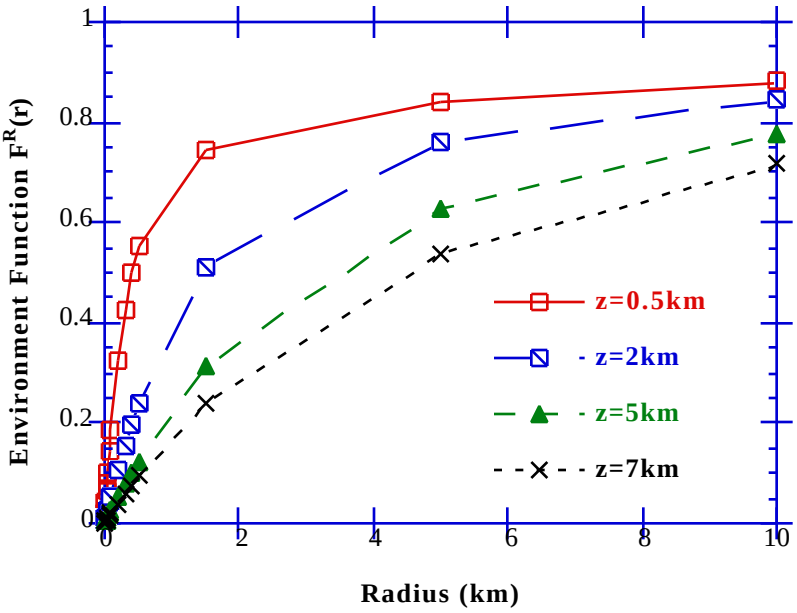

Figure 2: Variation of Rayleigh environment function wih sensor altitude.

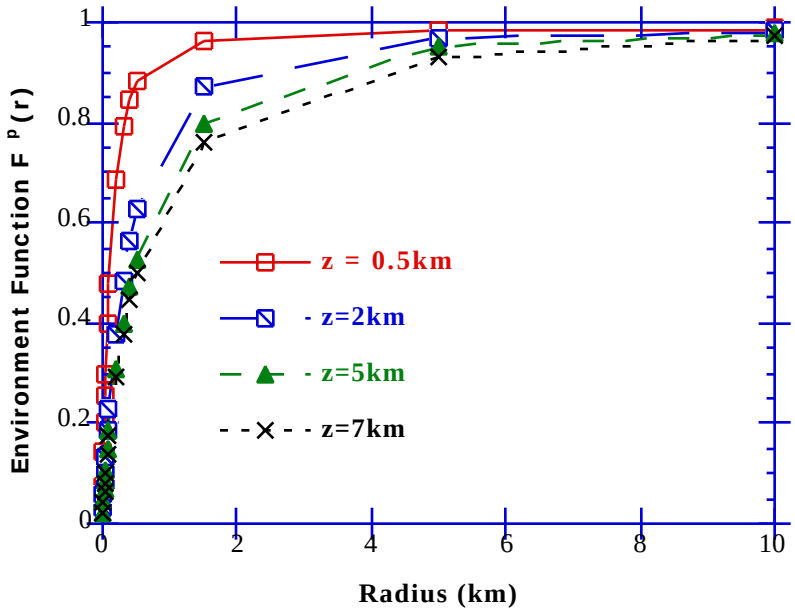

Figure 3: Same as figure 2 but for particles.

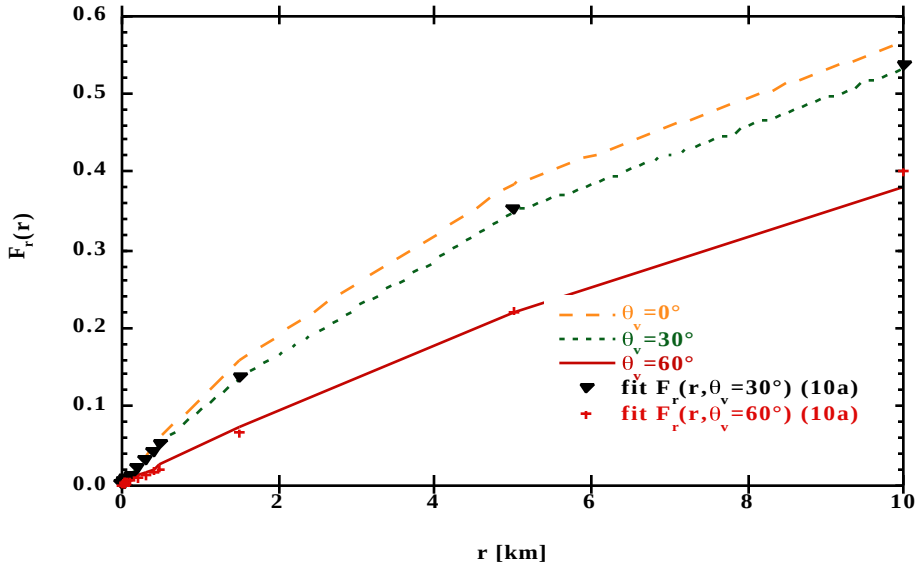

Figure 4a: Environment function for a pure molecular atmosphere (lines) for different view zenith angle (θ_V) compared to approximation used in 6S (symbols)

as a function of the distance to the imaged pixel (r).

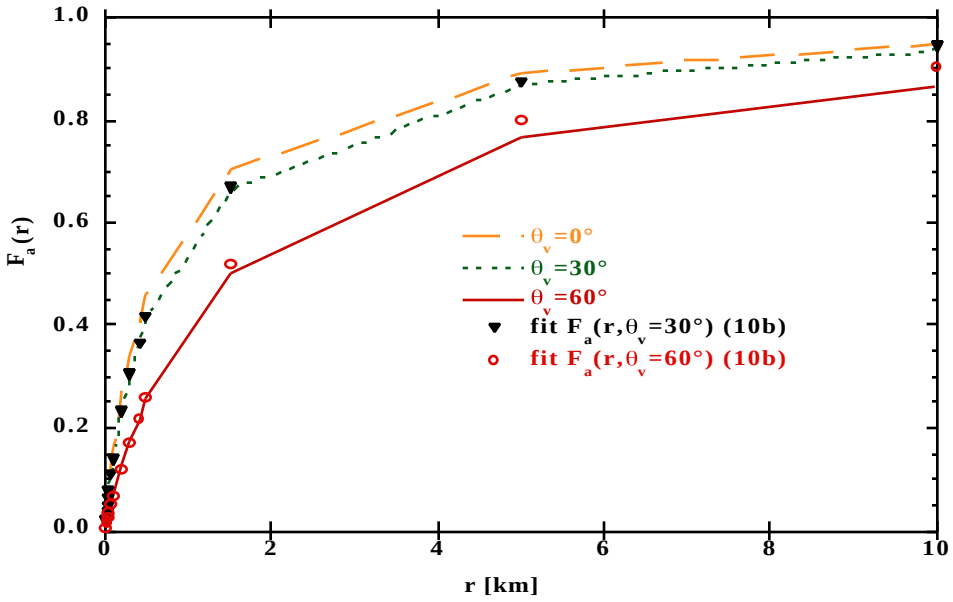

Figure 4b: same as Figure 4a but for aerosol.

SUBROUTINE GAUSS

Function: Compute for a given n, the gaussian quadrature (the n gaussian angles and the their respective weights). The gaussian quadrature is used in numerical integration involving the cosine of emergent or incident direction zenith angle.

SUBROUTINE INTERP

Function: To estimate the different atmospheric functions $\rho(\mu_S,\mu_v,\varphi_S,\varphi_v)$, $T(\theta)$ and s at any wavelength from the 10 discret computations (subroutine DISCOM).

Description: The different atmospheric functions (noted f) have been assumed linear as a function of optical depth τ, so the interpolation scheme is written,

$$f(\tau) = A\,\lambda^{-\alpha}$$

The constants A and α are interpolated between 0.4 and 3.7 μm and extrapolated for the two extreme intervals 0.25-0.4 and 3.7-4 μm.

The spectral dependances for Rayleigh ($\alpha = 4$) and aerosols ($\alpha = 1$) are quite different and we considered the two types of atmosphere separately .

SUBROUTINE ISO

Function: Compute the atmospheric transmission for either a satellite or aircraft observation as well as the spherical albedo of the atmosphere.

Description: The subroutine performs the computation on the basis of the Sucessive Orders of Scattering method (see subroutine OS). The transmission is obtained directly by initially setting the bottom of the atmosphere to a isotropic source of radiation. The spherical albedo is computed by numerical integration (gaussian quadrature) of the transmission function (see Eq. (01) of CSALBR.f).

SUBROUTINE KERNEL

Function: Compute the values of Legendre polynomials used in the successive order of scattering method.

SUBROUTINE MIE (and EXSCPHASE)

Function: To compute, using the scattering of electromagnetic waves by a homogeneous isotropic sphere, the physical properties of particles whose sizes are comparable to or larger than the wavelength, and to generate mixture of dry particles.

Description: The interaction of an electromagnetic wave with a absorbing sphere is described and expressed by the *Mie* theory *(Mie*, 1908). This theory has been particularly discussed by *Van de Hulst* (*Van de Hulst*, 1981) and also in part by many other authors (as example *Aden*, 1951; *Deirmendjian et al.*, 1961; *Wyatt*, 1962; *Kattawar and Plass*, 1967; *Dave*, 1969; *Hansen and Travis*, 1974; *Liou*, 1980). Here, we outline the basic equations of the *Mie* scattering behind the computation procedures.

1. Mie Scattering

Let λ represents the wavelength, r the radius of the sphere, x the *Mie*'s parameter ($x = 2\Pi r/\lambda$), m the complex index of refraction ($m = n_r - in_i$), and θ the direction of scattered radiation measured from the forward direction. From the *Maxwell*'s equations, we can defined two complex functions $S_1(x,m,\theta)$ and $S_2(x,m,\theta)$ related to the amplitude of the scattered radiation, respectively, perpendicular and parallel to the plane of scattering

$$S_1(x,m,\theta) = \sum_{n=1}^{\infty} \frac{(2n+1)}{n(n+1)} \left[a_n(x,m)\pi_n(\cos\theta) + b_n(x,m)\tau_n(\cos\theta) \right]$$

and

$$S_2(x,m,\theta) = \sum_{n=1}^{\infty} \frac{(2n+1)}{n(n+1)} \left[a_n(x,m)\tau_n(\cos\theta) + b_n(x,m)\pi_n(\cos\theta) \right]$$

1.1 *Computation of $a_n(x,m)$ and $b_n(x,m)$*

The complex functions $a_n(x,m)$ and $b_n(x,m)$ are given by

$$a_n(x,m) = \frac{\psi'_n(mx)\psi_n(x) - m\psi_n(mx)\psi'_n(x)}{\psi'_n(mx)\xi_n(x) - m\psi_n(mx)\xi'_n(x)}$$

and

$$b_n(x,m) = \frac{m\psi'_n(mx)\psi_n(x) - \psi_n(mx)\psi'_n(x)}{m\psi'_n(mx)\xi_n(x) - \psi_n(mx)\xi'_n(x)}$$

where the prime denotes derivative of the function with respect of the argument (*x* or *mx*), and where $\psi_n(z = x \text{ or } mx)$ and $\xi_n(z = x)$ are the *Ricatti-Bessel* functions defined by

$$\psi_n(z) = \left(\tfrac{1}{2}\Pi z\right)^{1/2} J_{n+1/2}(z) = z\, j_n(z)$$

$$\chi_n(z) = -\left(\tfrac{1}{2}\Pi z\right)^{1/2} N_{n+1/2}(z) = -z\, n_n(z)$$

$$\xi_n(z) = \left(\tfrac{1}{2}\Pi z\right)^{1/2} H^{(2)}_{n+1/2}(z) = z\, h^{(2)}_n(z) = \psi_n(z) + i\chi_n(z)$$

where $J_{n+1/2}$, $N_{n+1/2}$ and $H^{(2)}_{n+1/2}$ are respectively the *Bessel* functions of first, second, and third kind, and where j_n, n_n and $h^{(2)}_n$ are the corresponding spherical *Bessel* functions. $N_{n+1/2}$ is also called the *Neumann* functions and $H^{(2)}_{n+1/2}$ the half integral order *Hankel* function of the second kind.

In order to make the computational work more convenient, it is useful to introduce the logarithmic derivative of the *Ricatti-Bessel* functions (*Infeld*, 1947; *Aden*, 1951; *Kattawar and Plass*, 1967)

$$D_n(z) = \frac{d}{dz}\left[\ln \psi_n(z)\right]$$

$$G_n(z) = \frac{d}{dz}\left[\ln \xi_n(z)\right]$$

making use of these equations, $a_n(x,m)$ and $b_n(x,m)$ may be rewritten

$$a_n(x,m) = \frac{\psi_n(x)}{\xi_n(x)} \frac{D_n(mx) - mD_n(x)}{D_n(mx) - mG_n(x)}$$

and

$$b_n(x,m) = \frac{\psi_n(x)}{\xi_n(x)} \frac{mD_n(mx) - D_n(x)}{mD_n(mx) - G_n(x)}$$

Expressions of $a_n(x,m)$ and $b_n(x,m)$ are now reduced to a ratio of *Ricatti-Bessel* functions involving real arguments and a ratio of "$D_n(mx \text{ or } x)$ and $G_n(x)$" functions which are easily computable. We reported Figures 1 and 2, examples of $a_n(x,m)$ and $b_n(x,m)$ for m = 1.33 - i 0.001 and for x=10 and x=50 (which means respectively r ≈ 0.8 μm and r ≈ 4.0μm at 0.50 μm).

Also in order to save time, we use in 6S the criterion defined by *Deirmendjian et al.,* 1961:

"*the quantities* a_n *and* b_n *are terminated either when* $(a_n\, a_n^* + b_n\, b_n^*)/\, n \;<\; 10^{-14}$"

1.1.1 *Computation of the Ricatti-Bessel function.*

The ratio of *Ricatti-Bessel* functions can be reduced to a ratio of spherical *Bessel* functions with a real argument *x* as follow

$$\frac{\psi_n(x)}{\xi_n(x)} = \frac{j_n(x)}{h^{(2)}_n(x)} = \frac{j_n(x)}{j_n(x) - in_n(x)}$$

The spherical *Bessel* functions $j_n(x)$, $n_n(x)$ or $h^{(2)}_n(x)$, have different behaviors following they are below or above the transition line defined by $x^2 = n(n+1)$. Below the transition line

($n(n+1) < x^2$), they behave as oscillating functions of both order and argument, whereas the behavior becomes monotonic above the transition line ($n(n+1) > x^2$).

It has been shown by many authors that $n_n(x)$ or $h_n^{(2)}(x)$ can be processed using an upward recurrence (what ever values of *n* and *x*). Functions $n_n(x)$ are computed using

$$n_{n+1}(x) = \frac{2n+1}{x} n_n(x) + n_{n-1}(x)$$

with $$n_0(x) = -\frac{cos(x)}{x} \qquad n_1(x) = -\frac{cos(x)}{x^2} - \frac{sin(x)}{x}$$

Figures 03 show examples of the $n_n(x)$ function for x=10 and x=50.

For $j_n(x)$, we use a similar recurrence

$$j_{n+1}(x) = \frac{2n+1}{x} j_n(x) + j_{n-1}(x)$$

but, has it is explained in the paper of *Corbató and Uretsky*, 1959, the function $j_n(x)$ cannot be computed by an upward recurrence "*since upward recursion (except in the region of the x-n plane where j_n oscillate) would bring about a rapid loss of accuracy*". Then, a downward recurrence is called for, but we have to define the starting value of *n*, and for that purpose we use the work of *Corbato and Uretsky* which is summurized hereafter. Let *N* be the starting order of the recursion with $N(N+1) > x^2$, in their paper, they show "*that rather than accurately evaluate $j_N(x)$ and $j_{N-1}(x)$ to start the process, a very approximately starting the recursion at a higher order will give a set of numbers which are accurately proportional to the j_n over the desired range of n from 0 to N*". Let $\bar{j}_n$ be one of these numbers.

They propose to define the higher order ν by

$$\nu = N' - \frac{ln\varepsilon_N}{ln2}\left[A + \frac{B\,u'(2-u'^2)}{2(1-u'^2)}\right]$$

where *A*=0.10 and *B*=0.35,

$\varepsilon_N = 2^{-30}$ (this value comes from the fact that generally computers can store floating points numbers with a 30 binary digit mantissa),

and $u' = 2x/(2N' + 1)$ with $N' = N$ or $N' = x - \frac{1}{2} + \sqrt{-\frac{ln\varepsilon_N}{ln2} Bx}$ such that ν be the lower, with however $N' \geq N$.

To avoid computational difficulties above the transition line, *Corbato and Uretsky* worked with the ratio $\bar{r}_n = \bar{j}_{n+1}/\bar{j}_n$ using the recurrence relation

$$\bar{r}_{n-1} = \frac{x}{2n+1-x\bar{r}_n}$$

with the starting condition $\bar{r}_\nu = 0$. The recursion is continued downward until a ratio $\bar{r}_n$ which exceeds unity is reached. Then, they set $\bar{j}_{n+1} = \bar{r}_n$ and $\bar{j}_n = 1$, and continue downward using the recurrence relation

$$\bar{j}_{n-1}(x) = \frac{2n+1}{x}\bar{j}_n(x) + \bar{j}_{n+1}(x)$$

The positive number $\bar{j}_n$ is defined by $\bar{j}_n(x) = \alpha\ j_n(x)$ with α a constant of proportionality obtained from the relation

$$\alpha = (\bar{j}_0(x) - x\bar{j}_1(x))\cos(x) + x\bar{j}_0(x)\sin(x)$$

Figures 03 also show examples of the $j_n(x)$ function for x=10 and x=50.

1.1.2 *Computation of the $D_n(mx\ or\ x)$ and $G_n(x)$ function.*

As *Kattawar and Plass*, 1967, have pointed out, the procedure of computing $D_n(z)$ by an upward recurrence is unstable, then a downward process is needed, and $D_n(z)$ is defined using

$$D_{n-1}(z) = n/z - \frac{1}{D_n(z) + n/z}$$

Calculations have to be started at an order $n = \nu' >> |z|$ with a starting value which is not really important because the serie converges rapidly to the exact value (then $D_{\nu'}(z) = 0$ is a convenient value). When $n < |z|$, $D_n(z)$ becomes oscillatory, and then there is no problem for the calculation in using the recurrence relation. For practical reasons, we selected in 6S $\nu' = \nu$ as defined for j_n.

Kattawar and plass have also shown that $G_n(x)$ may always be calculated using an upward process with a starting value $G_0(x) = -i$

$$G_n(x) = -n/x - \frac{1}{G_{n-1}(x) - n/x}$$

Figure 04 reportes examples of the $D_n(x)$ function, Figures 05 the $D_n(mx)$ function, and Figures 06 the $G_n(x)$ function.

1.2 <u>*Computation of $\pi_n(\cos\theta)$ and $\tau_n(\cos\theta)$*</u>

Functions π_n and τ_n depend of only the scattering angle θ. They are related to the associated *Legendre* polynomials $P_n^1(\cos\theta)$

$$\pi_n(\cos\theta) = \frac{1}{\sin\theta} P_n^1(\cos\theta)$$

$$\tau_n(\cos\theta) = \frac{d}{d\theta} P_n^1(\cos\theta)$$

and are computed from upward recurrence relations defined as follow

$$n\,\pi_{n+1}(\cos\theta) = (2n+1)\cos\theta\ \pi_n(\cos\theta) - (n+1)\ \pi_{n-1}(\cos\theta)$$

$$\tau_{n+1}(\cos\theta) = (n+1)\cos\theta\ \pi_{n+1}(\cos\theta) - (n+2)\ \pi_n(\cos\theta)$$

with the starting values

$$\pi_0(\cos\theta) = 0 \quad \pi_1(\cos\theta) = 1$$

Examples of functions π_n and τ_n are shown Figures 07 for n=1 to 6 and for 0°<θ<90°.

2. Computation of the physical properties of a particle (see for example Liou, 1980).

2.1 *Extinction*

The **extinction cross section** σ_e, which denotes the amount of energy removed (scattered and absorbed) from the original beam by the particle, is obtained considering a point in the forward direction (θ=0) in the "far field". If we consider an isotropic homogeneous sphere, the extinction cross section is given by

$$\sigma_e(\lambda,r,m) = \frac{4\Pi}{(2\Pi/\lambda)^2} \quad {}_e[S(x,m,\theta = 0)]$$

with

$$S(x,m,\theta = 0) = S_1(x,m,\theta = 0) = S_2(x,m,\theta = 0) = \frac{1}{2}\sum_{n=1}^{\infty}(2n+1)[a_n(x,m) + b_n(x,m)]$$

Thus the **extinction efficiency** Q_e is defined by

$$Q_e(\lambda,r,m) = \frac{\sigma_e(\lambda,r,m)}{\Pi r^2} = \frac{2}{x^2}\sum_{n=1}^{\infty}(2n+1)\Re_e[a_n(x,m) + b_n(x,m)]$$

2.2 *Scattering*

The **scattering cross section** σ_s is derived by a similar way, but considering a scattered light in an arbitrary direction, by

$$\sigma_s(\lambda,r,m) = \frac{\Pi}{(x/r)^2}\int_0^{\Pi}[S_1(x,m,\theta)S_1^*(x,m,\theta) + S_2(x,m,\theta)S_2^*(x,m,\theta)]\sin\theta\, d\theta$$

Owing of the functions π_n and τ_n, we have to integrate products of the associated *Legendre* polynomials. Using the orthogonal and recurrence properties of these polynomials, the scattering cross section can be written

$$\sigma_s(\lambda,r,m) = \frac{2\Pi}{(x/r)^2}\sum_{n=1}^{\infty}(2n+1)[a_n(x,m)a_n^*(x,m) + b_n(x,m)b_n^*(x,m)]$$

where the asterisk denotes the complex conjugate value, and the **scattering efficiency** Q_s can be evaluated by the relation

$$Q_s(\lambda,r,m) = \frac{\sigma_s(\lambda,r,m)}{\Pi r^2} = \frac{2}{x^2}\sum_{n=1}^{\infty}(2n+1)[a_n(x,m)a_n^*(x,m) + b_n(x,m)b_n^*(x,m)]$$

2.3 *Absorption*

The **absorption cross section** σ_a and the **absorption efficiency** Q_a can be deduced from

$$\sigma_a(\lambda,r,m) = \sigma_e(\lambda,r,m) - \sigma_s(\lambda,r,m) \qquad Q_a(\lambda,r,m) = Q_e(\lambda,r,m) - Q_s(\lambda,r,m)$$

2.4 *Phase function*

On the basis of the *Stokes* parameters, the intensity *I* of the electromagnetic waves at each point and in any given direction can be related to the incident intensity I_0 *by*

$$I = M_{11}\, I_0$$

with

$$M_{11}(\lambda,r,m,\theta) = \frac{1}{2x^2}[S_1(x,m,\theta)S_1^*(x,m,\theta) + S_2(x,m,\theta)S_2^*(x,m,\theta)]$$

The angular distribution of the scattered energy for a single sphere (also called **Phase function**) $P_{11}(\lambda, r,m,\theta)$ can be defined by

$$M_{11}(\lambda,r,m,\theta) = \frac{\sigma_s(\lambda,r,m)}{4\Pi\, r^2}\, P_{11}(\lambda,r,m,\theta)$$

then

$$P_{11}(\lambda,r,m,\theta) = \frac{2\Pi}{(x/r)^2\,\sigma_s(\lambda,r,m)}[S_1(x,m,\theta)S_1^*(x,m,\theta) + S_2(x,m,\theta)S_2^*(x,m,\theta)]$$

It can be check that

$$\int_0^{2\Pi}\int_0^{\Pi} P_{11}(\lambda,r,m,\theta)\, \sin\theta\, d\theta\, d\phi = 4\Pi$$

3. Physical properties of a sample of identical particles

We now consider a sample of identical particles whose size is described by the **size distribution** *n(r)* (in $cm^{-3}\ \mu m^{-1}$) such that

$$\int_0^{\infty} n(r)\, dr = \int_0^{\infty} \frac{dN(r)}{dr}\, dr = 1$$

where *d N(r)* represents the number of particle per unit volume having a radius between *r* and *r+dr*.

In 6S, we selected several possibilities to represent the size distribution, thus the user will be allowed to choice between 4 options:

1- a Junge power-law function. *Junge,* 1952, showed that the size distribution of aerosols whose radii are larger than 0.1μm may be described by

$$\frac{dN(r)}{d\log r} = \ln(10)\, c\, r_0^{\alpha} \left(\frac{r_0}{r}\right)^{\alpha-1} \quad \text{or} \quad \frac{dN(r)}{dr} = c\, r_0^{\alpha} \left(\frac{r_0}{r}\right)^{\alpha}$$

with α varying between 3 and 5, c the number density of particles with radius r_0 and r_0 an arbitrary radius.

Figure 08-a shows an example of Junge Power-Law function which is the "Model C" defined by *Deirmendjian,* 1969, for $c.r_0^{\alpha}=1$ and α=4

2- a Modified Gamma distribution function. Used by *Deirmendjian*, 1964, to compute scattering properties of water clouds and haze and to fit aerosol measurements. Also employed by Mie in the *Mie* and diffraction calculations.

$$\frac{dN(r)}{dr} = A\left(r/r_0\right)^{\alpha} \; exp\left(-b\left(r/r_0\right)^{\gamma}\right) \qquad \text{with } r_0=1\mu m$$

An example of Modified Gamma distribution function is given Figure 08-b (Volcanic Ash defined in WCP 112, A=5461.33, α=1.0, γ=0.5, b=16).

3- a Log-Normal distribution function. Based on the *Junge* power-law function, *Davies*, 1974, introduced this function to take into account large particles.

$$\frac{dN(r)}{dlogr} = \frac{N}{\sqrt{2\Pi}\; log\sigma} \; exp\left(-\frac{1}{2}\left(\frac{log\, r - log\, r_M}{log\, \sigma}\right)^2\right)$$

where r_M is the mean radius of the particle, and σ the standard deviation of *r*.

We reported Figure 08-c examples of Log-Normal distribution functions which are the 3 three components of the "Continental Model" defined in WCP 112 (see AEROSO to find r_M and σ).

4- sun photometer measurements. You enter directly $d\,V(r)/\,dlogr \approx r^4 dN(r)/dr$.

The Figure 09 shows the same function than Figures 08 but for dV(r)/dlog(r).

Under the assumption of "independent scattering" which means that particles are sufficiently far from each other compared to the incident wavelength to consider just one scattering, it is possible to add scattered intensities independently of the phase of the wave. Then we can defined the radiative characteristics upon the particle size distribution by

•The **extinction** (e), **scattering** (s) and **absorption** (a) coefficient

$$k_{e,s,a}(\lambda,m) = \int_{r_{min}}^{r_{max}} Q_{e,s,a}(\lambda,r,m)\; \Pi\; r^2 \frac{dN(r)}{dr}\, dr$$

•The **normalized phase function**

$$P(\lambda,m,\theta) = \frac{1}{k_s(\lambda,m)} \int_{r_{min}}^{r_{max}} M_{11}(\lambda,r,m,\theta)\; 4\Pi r^2 \frac{dN(r)}{dr}\, dr$$

•We now introduce the **single scattering albedo** ω_0 which represents the percentage of energy removed from the incident beam which will reappear as a single scattered radiation.

$$\omega_0(\lambda,m) = \frac{k_s(\lambda,m)}{k_e(\lambda,m)}$$

Computationally, $k_{e,s,a}(\lambda,m)$ and $P(\lambda,m,\theta)$ are integrated step by step following:

$$k_{e,s,a}(\lambda,m) = \sum_{r_{\min}}^{r_{\max}} Q_{e,s,a}(\lambda,r,m)\ \Pi\ r^2 \frac{dN(r)}{dr} \Delta r$$

and

$$P(\lambda,m,\theta) = \frac{1}{k_s(\lambda,m)} \sum_{r_{min}}^{r_{max}} M_{11}(\lambda,r,m,\theta)\ 4\Pi r^2 \frac{dN(r)}{dr} \Delta r\,,$$

where Δr is defined by

$$log\left(\frac{r + \Delta r}{r}\right) = 0.03$$

The value 0.03 has been selected in order to preserve a good accuracy with a reasonable computational time. For example *D'Almeida* used a very small step width, 0.011, for the computations given in his book (*D'Almeida et al.*, 1991). The logarithmic expression of Δr comes from the fact that size distributions can be frequently described by a logarithmic shape (*Junge*, 1952; *Davies*, 1974).

Finally, and, in order to save computational time, we defined a criterion on the summation such that the computations are not performed either when

$$\left(\frac{n_i}{n}\ \Pi\ r^2 \frac{dN(r)}{dr} \Delta r\right) \frac{1}{\sqrt{\lambda}} < 10^{-8}$$

where n_i/n is the percentage density of particles (cf. subroutine AEROSO for some examples). The latter criterion has been tested between 0.4 and 4.0 µm.

4. Physical properties of a mixture of aerosol type

We now consider a mixture of particles originating from different sources (4 max.). The mixing is treated in the same way that the one used to generated the data base in the AEROSO subroutine.

Let us recall that the mixture of individual components (or type) of an aerosol is characterized by the percentage density of particles n_i/n, and if we assume that the particles are spherical, each type i is described by its size distribution (then by its microphysical identity: r_{Mi} and σ_i see Table 1 for some examples (*Shettle and Fenn*, 1976; *World Climate Programme*, 1986), and by its complex refractive index m_i (see Table 2, from (*Shettle and Fenn*, 1976; *Shettle and Fenn*, 1979; *World Climate Programme*, 1986; *D'Almeida et al.*, 1991). For the size distribution, the Log-Normal distribution is well adapted to emphasize the individual components of a mixture (*Davies*, 1974, *D'Almeida et al.*, 1991).

5. Examples and comparisons

The comparison of the computed normalized at 550 nm K_e, K_s and ω_0 values that obtained by 6S with those given by *World Climate Programme*, 1986 are reported for a Continental and an Urban dry aerosol model respectively Table 3 and Table 4. Also reported in theses tables, are the asymmetry parameters g. In 6S, this parameter is already computed in an another subroutine, but we can compute it here using

$$g = \frac{\int_{-1}^{+1} \cos\theta \; P(\lambda, m, \theta)\, d\cos\theta}{\int_{-1}^{+1} P(\lambda, m, \theta)\, d\cos\theta}$$

The comparison of the phase function of a Continental model (WMO/WCP-112) computed by the MIE subroutine with those by a precise code (AEROSO subroutine) is reported Figure 10 for several wavelengths. Also, we show, Figure 11, the phase function computed using the volumic distribution dV/dlogr provided by a CIMEL sunphotometer during the SCAR-A field experiment (Sulfate Clouds Aerosol and Reflectances - America) that took place in July 1993 in the Eastern USA.

The parameters are:

For IAER=8 Multimodal Log Normal (up to 4 modes)

r_{min},r_{max},icp

then for k=1 to icp, enter:

σ, r_M, C_{ij}

$r_n(\lambda_j)$, j=1,10

$r_i(\lambda_j)$, j=1,10

where r_{min} and r_{max} are the radii min and max of the aerosol

icp the number of mode (component)

σ and r_M are parameters of the Log-Normale size distributions

Cij is the percentage density of particles (see SUBROUTINE AEROSO)

r_n and r_i are the real and imaginary index of refraction of each component

with $r=r_n-i\ r_i$. You have to enter these parameters for the 10 wavelengths

used to compute the atmospheric signalwhich are:

0.400, 0.488, 0.515, 0.550, 0.633, 0.694, 0.860, 1.536, 2.250, 3.750

For IAER=9 Modified gamma distribution

r_{min},r_{max}

α, b, γ

$r_n(\lambda_j)$, j=1,10

$r_i(\lambda_j)$, j=1,10

where α, b, and γ are the parameters of the Modified Gamma size distribution

For IAER=10 Junge Power-Law distribution

r_{min},r_{max}

α

$r_n(\lambda_j)$, j=1,10

$r_i(\lambda_j)$, j=1,10

where α is the parameter of the Junge Power-Law size distribution

For IAER=11 Sun Photometer distribution (50 values max)

irsunph

for k=1 to irsunph enter: r and dV/dlogr

$r_n(\lambda_j)$, j=1,10

$r_i(\lambda_j)$, j=1,10

where irsunph is the number of value and dV/dlogr is usually profided by sunphotometers.

Table 1: Microphysical characteristics of the aerosol type (dry particles) used for the comparisons shown Tables 3 and 4 (from WMO-WCP112).

	Dust-Like	Water Soluble	Oceanic	Soot
r_{Mi} (μm)	0.500	0.0050	0.30	0.0118
σ_i	2.990	2.990	2.51	2.00

Table 2: Complexe refractive indexes of the aerosol types (dry particles) used for the comparisons shown Tables 3 and 4 (from WMO-WCP112).

λ	Dust-Like		Water Soluble		Oceanic		Soot	
(μm)	n_r	n_i	n_r	n_i	n_r	n_i	n_r	n_i
0.400	1.530	8.00E-3	1.530	5.00E-3	1.385	9.90E-9	1.750	0.460
0.488	1.530	8.00E-3	1.530	5.00E-3	1.382	6.41E-9	1.750	0.450
0.515	1.530	8.00E-3	1.530	5.00E-3	1.381	3.70E-9	1.750	0.450
0.550	1.530	8.00E-3	1.530	6.00E-3	1.381	4.26E-9	1.750	0.440
0.633	1.530	8.00E-3	1.530	6.00E-3	1.377	1.62E-8	1.750	0.430
0.694	1.530	8.00E-3	1.530	7.00E-3	1.376	5.04E-8	1.750	0.430
0.860	1.520	8.00E-3	1.520	1.20E-2	1.372	1.09E-6	1.750	0.430
1.536	1.400	8.00E-3	1.510	2.30E-2	1.359	2.43E-4	1.770	0.460
2.250	1.220	9.00E-3	1.420	1.00E-2	1.334	8.50E-4	1.810	0.500
3.750	1.270	1.10E-2	1.452	4.00E-3	1.398	2.90E-3	1.900	0.570

Table 3: Comparison between 6S and WMO-WCP112

for a Continental model (normalized value-dry particles)

	K_{ext}		K_{sca}		ω_0		g	
λ	6S	WMO	6S	WMO	6S	WMO	6S	WMO
0.400	1.40	1.40	1.27	1.27	0.902	0.901	0.643	0.646
0.488	1.14	1.14	1.03	1.03	0.900	0.898	0.637	0.640
0.515	1.08	1.08	0.967	0.967	0.899	0.897	0.635	0.638
0.550	1.00	1.00	0.893	0.891	0.893	0.891	0.634	0.637
0.633	0.849	0.849	0.755	0.754	0.890	0.888	0.629	0.633
0.694	0.760	0.760	0.671	0.669	0.881	0.879	0.628	0.631
0.860	0.577	0.577	0.487	0.486	0.844	0.841	0.629	0.633
1.536	0.282	0.283	0.212	0.212	0.753	0.750	0.641	0.645
2.250	0.150	0.151	0.115	0.115	0.765	0.761	0.738	0.741
3.750	0.101	0.103	0.0796	0.0805	0.790	0.785	0.777	0.779

Table 4: Comparison between 6S and WMO-WCP112

for an urban model (normalized value-dry particles)

	K_{ext}		K_{sca}		ω_0		g	
λ	6S	WMO	6S	WMO	6S	WMO	6S	WMO
0.400	1.48	1.48	0.980	0.976	0.664	0.660	0.600	0.600
0.488	1.16	1.17	0.766	0.762	0.658	0.654	0.594	0.593
0.515	1.09	1.09	0.715	0.711	0.655	0.651	0.592	0.592
0.550	1.00	1.00	0.651	0.647	0.651	0.647	0.591	0.591
0.633	0.828	0.829	0.535	0.532	0.646	0.641	0.587	0.587
0.694	0.733	0.733	0.466	0.462	0.635	0.631	0.585	0.585
0.860	0.542	0.542	0.322	0.319	0.593	0.588	0.584	0.583
1.536	0.242	0.243	0.111	0.111	0.460	0.455	0.564	0.565
2.250	0.123	0.124	0.0428	0.0426	0.347	0.342	0.583	0.585
3.750	0.0647	0.0659	0.0177	0.0181	0.274	0.274	0.579	0.587

Figures 01: Examples of a $a_n(m,x)$ function.

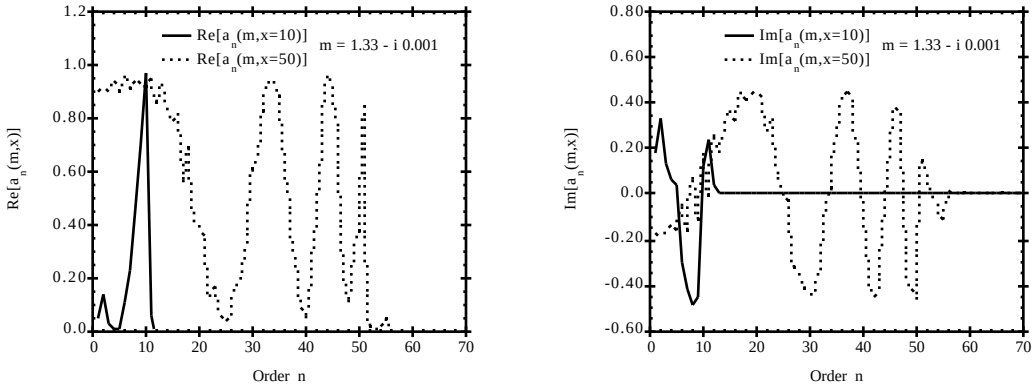

Figures 02: Examples of a $b_n(m,x)$ function.

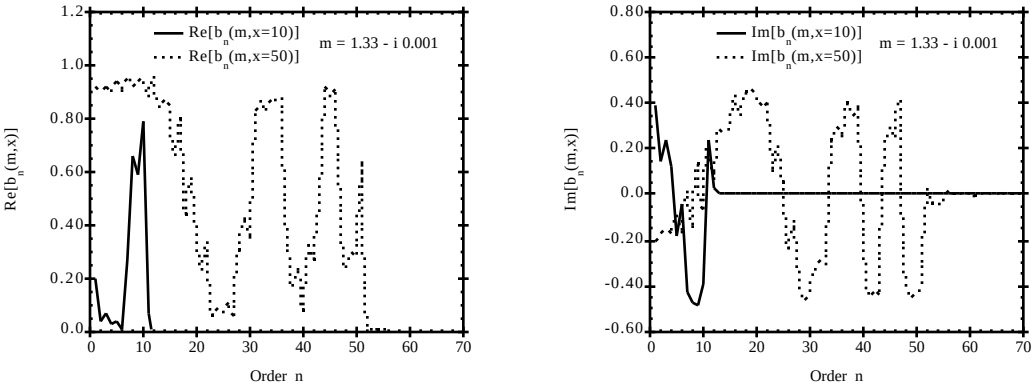

Figures 03: Examples of spherical Bessel functions $j_n(x)$ and $n_n(x)$

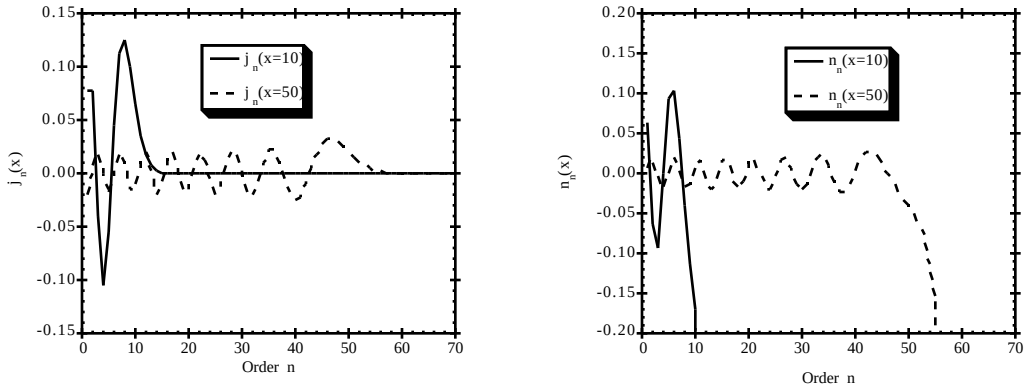

Figure 04: Examples of a $D_n(x)$ function.

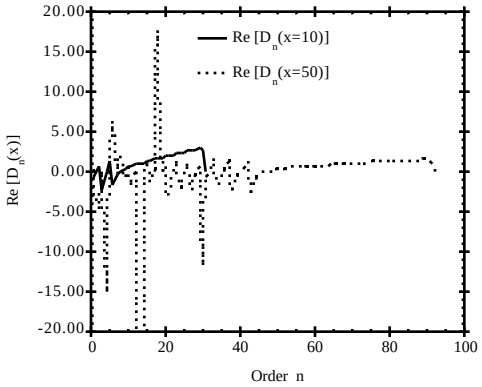

Figures 05: Examples of a $D_n(mx)$ function.

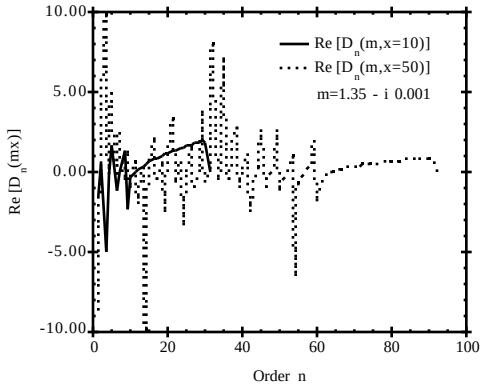

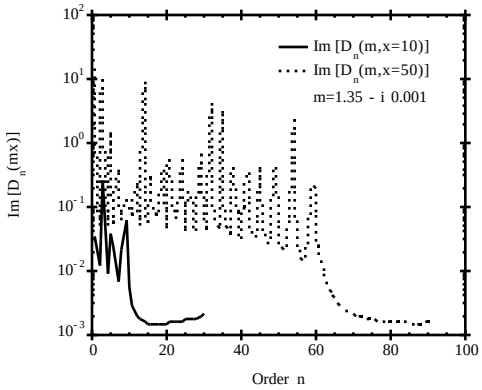

Figures 06: Examples of a $G_n(x)$ function.

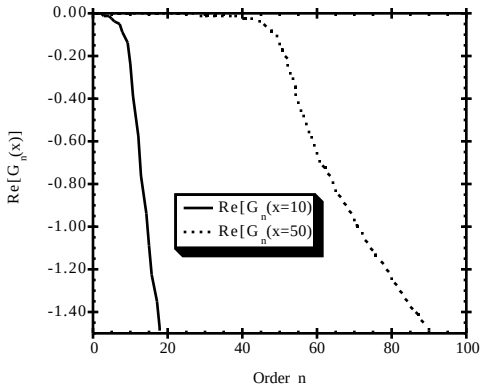

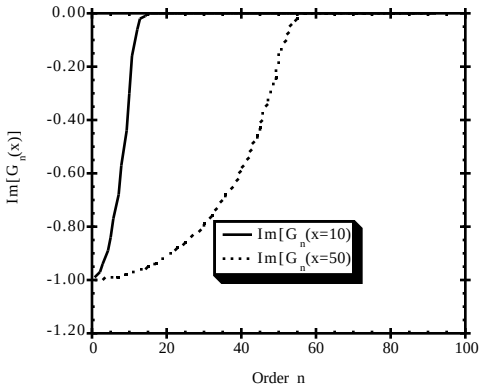

Figures 07: Examples of functions $\Pi_n(\theta)$ and $\tau_n(\theta)$ for n=1 to 6.

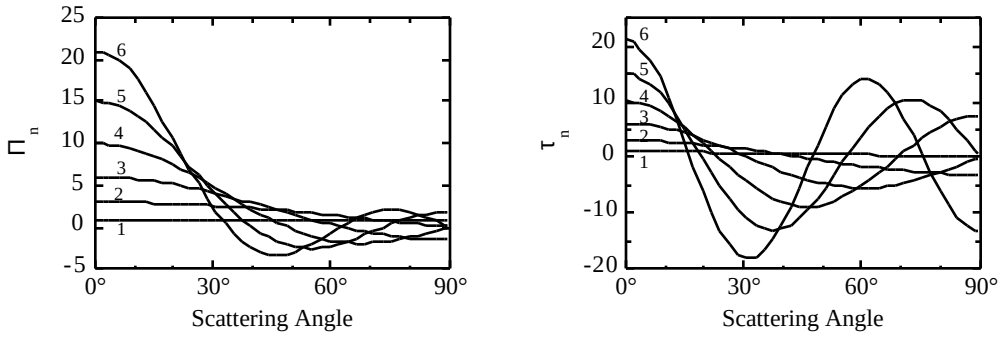

Figure 08-a: Junge Power-law function: Model C (Deirmendjian, 1954)

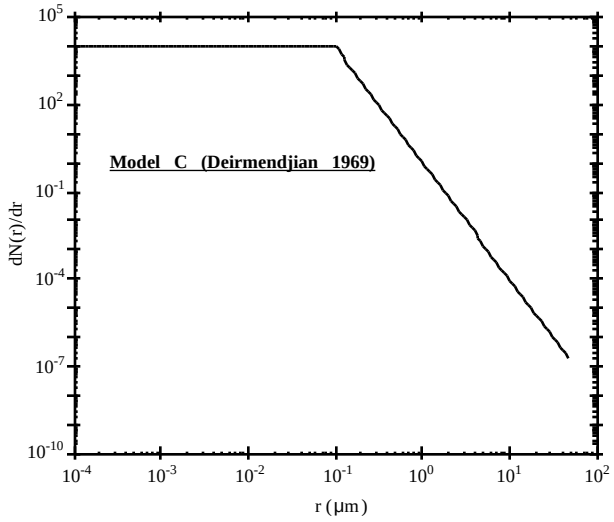

Figure 08-b: Modified Gamma distribution function: Volcanic Ash (WCP 112)

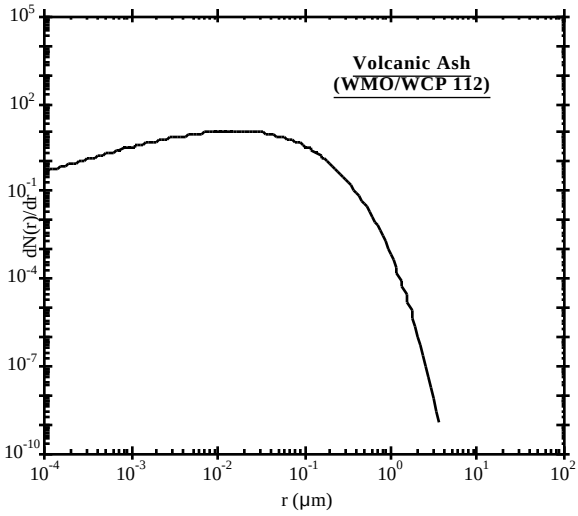

Figure 08-c: Log-Normal distribution function: Continental Model (WCP 112)

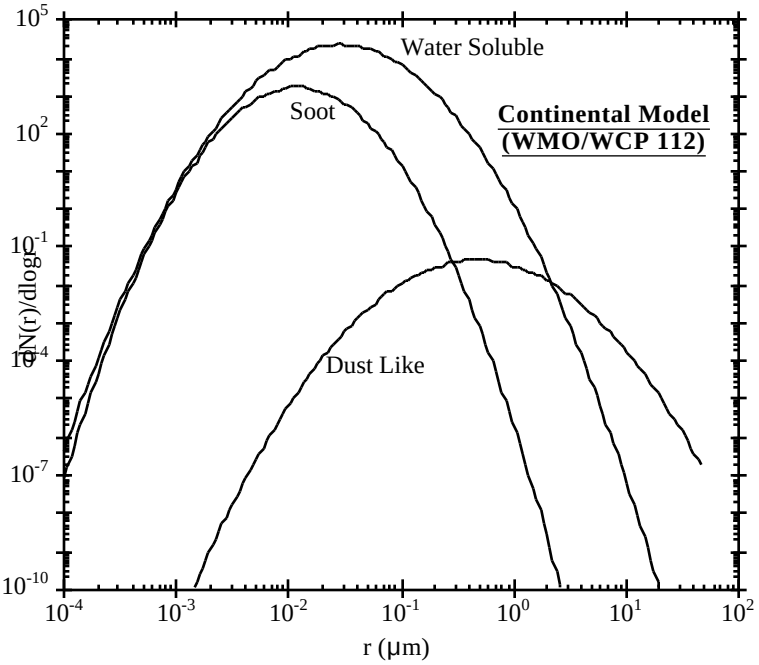

Figure 09: Same as Figures 8 but represented for dV/dlogr

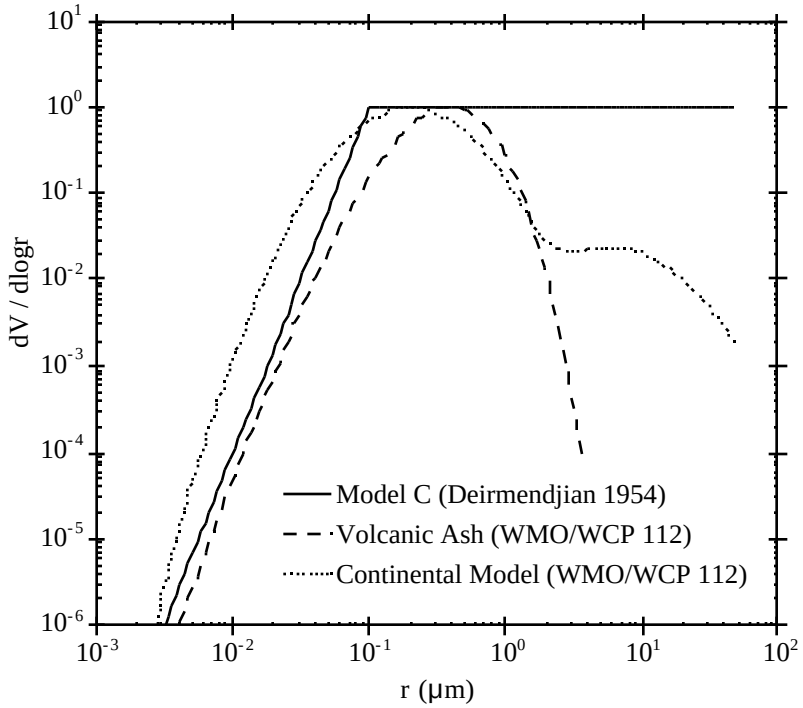

Figure 10: Phase function (dry particle) as computed by the MIE subroutine and by the one generated by AEROSO subroutine (exact case).

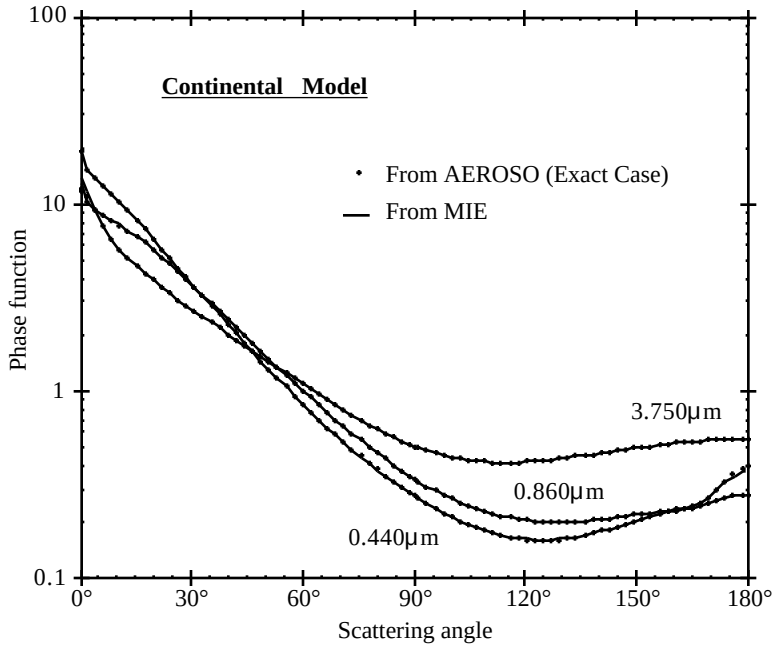

Figure 11: Phase function as computed by MIE subroutine using the dV/dlogr provided by a sunphotometer CIMEL during the SCAR-A experiment (Hog Island, July 11, 1993).

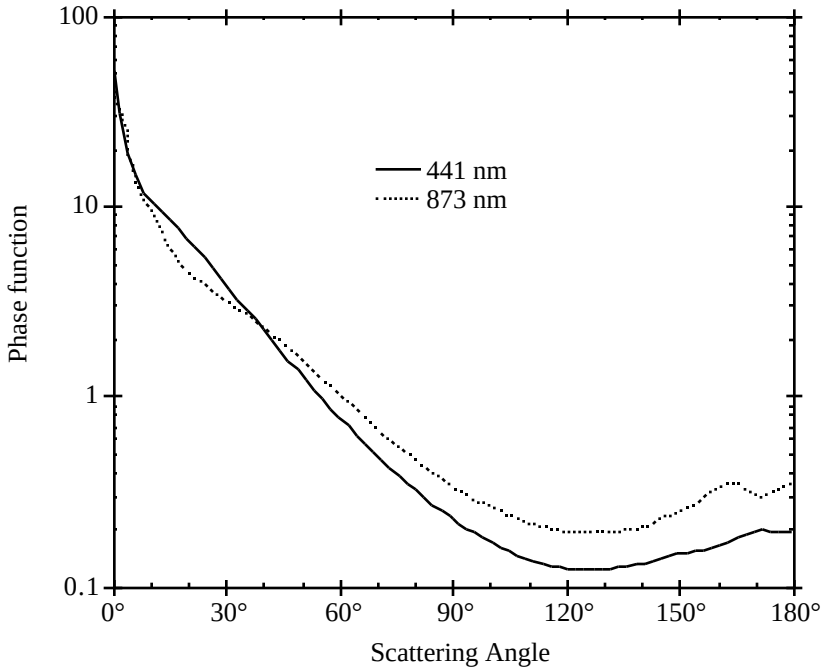

REFERENCES

A.L. ADEN, Electromagnetic Scattering from Spheres with Sizes Comparable to the Wavelength. *J. Appl. Phys.*, 22, 5, 601-605, 1951

F.J. CORBATO and J.L. URETSKY, Generation of Spherial Bessel Functions in Digital Computers. *J. Assoc. Computing Machinery*, 6, 366-375, 1959

G.A. D'ALMEIDA, P. KOEPKE, and E.P. SHETTLE, Atmospheric Aerosols Global Climatology and Radiative Characteristics, A. Deepak Publishing, Hampton, 1991.

J.V. DAVE, Scattering of Visible Light by Large Water Spheres. *Appl. Opt.*, 8, 1, 155-164, 1969

C.N. DAVIES, Size distribution of atmospheric particles. *J. Aerosol Sci.*, 5, 293-300, 1974

D. DEIRMENDJIAN, Scattering and Polarization properties of water clouds and hazes in the visible and infrared. *Appl. Opt.*, 3, 187-196, 1964

D. DEIRMENDJIAN, R. CLASEN, and W. VIEZEE, Mie Scattering with Complex Index of Refraction. *J. Opt. Soc. Am.*, 51, 6, 620-633, 1961

D. DEIRMENDJIAN, Electromagnetic scattering on spherical polydispersion. Elsevier Ed. New-York, 1969

J.E. HANSEN and L. TRAVIS, Light scattering in planetary atmospheres. *Space Sci. Rev.*, 16, 527-610, 1974

L. INFELD, The Influence of the Width of the Gap upon the Theory of Antennas. *Quart. Appl. Math.*, 5, 2, 113-132, 1947

C.E. JUNGE, Gesetzmäßigkeiten in der Droßenverteilung atmosphärischer Aerosole über dem Kontinent. *Ber d. Deirsch Wetterdienst U.S.-Zone*, 35, 261-277, 1952

G.W. KATTAWAR and G.N. PLASS, Electromagnetic Scattering from Absorbing Spheres. *Appl. Opt.*, 6, 8, 1377-1382, 1967

K.N. LIOU, An Introduction to Atmospheric Radiation, Academic Press Inc., San Diego, 1980.

G. MIE, Beigrade zur Optik trüber Medien, speziell kolloidaler Metallösungen. *Ann. Physik.*, 25, 377-445, 1908

E.P. SHETTLE and R.W. FENN, Models of atmospheric aerosols and their optical properties, in: *Optical Properties in the Atmosphere*, AGARD-Cp-183, NTIS, ADA 028615, 1976.

E.P. SHETTLE and R.W. FENN, Models for the aerosol of the lower atmosphere and the effect of humidity variations on their optical properties, AFGL-TR-79-0214, *Environmental Research Paper No 675*, NTIS, ADA 085951, 1979.

H.C. VAN DE HULST, Light Scattering by Small Particles, Dover Publications, New York, Dover, 1981.

WORLD CLIMATE PROGRAMME, WCP-55, Report of the expert meeting on aerosols and their climatic effects (Eds. A. Deepak and H.E. Gerber), World Meteorological Organization, Geneva, 1983.

WORLD CLIMATE PROGRAMME, WCP-112, A preliminary cloudless standard atmosphere for radiation computation, World Meteorological Organization, *WMO/TD-No 24*, Geneva, 1986.

P.J. WYATT, Scattering of Electromagnetic Plane Waves from Inhomogeneous Spherically Symmetric Objects. *Phys. Rev.*, 127, 5, 1837-1843, 1962

SUBROUTINE ODA550

Function: To compute the extinction cross section and the aerosol optical depth at λ = 550 nm from the vertical distributions of the particle density (in particules/cm^3).

Description: We have considered the 2 profiles, suggested by *Mc Clatchey et al* (1971), corresponding to a visibility of 23 (clear) and 5 *km* (hazy) at ground level. The total numbers of aerosols for the clear atmosphere have been adjusted so that the total extinction coefficient at λ = 550 nm becomes identical to the values used by *Elterman* (1964).

This total extinction coefficient K (in km^{-1}) is obtained from

$$K^{550}(z) = \sigma_{550}\, 10^{-3}\, N(z)$$

where s is the extinction cross section in mm2 and N(z) the particules density (in part/cm3) (the factor 10^{-3} is to obtain an extinction coefficient in km^{-1}). σ was computed with the same aerosol model as the one defined by *Mc Clatchey*, index of refraction equal to 1.50 and size distribution similar to *Deirmendjian's* model "C" (1969) (cut off has been extended from 5 to 10 μm). The computed value of σ_{550} is 0.056032.

The optical thickness τ is defined by

$$\tau_{550} = \int_0^{+\infty} K^{550}(z)\, dz$$

We obtain the optical thicknesses at 550 nm, 0.235 and 0.780 respectively for the two standard visibilities 23 and 5*km*. For another visibility, we compute a new profile particle density from those defined for 23 and 5*km*. The calculations were made using the following interpolations,

$$N(z) = \frac{a(z)}{VIS} + b(z)$$

We obtain for example :

$\tau = 0.152$ for V = 50*km*,
$\tau = 0.520$ for V = 8*km*.

Reference :

R.A. Mc CLATCHEY, R.W. FENN, J.E.A. SELBY, F.E. VOLZ, J.S. GARING. Optical properties of the Atmosphere (revised), AFCRL 71-0279, Env. Research Paper 354, Bedford, Massachusetts, U.S.A., 1971.

D. DEIRMENDJIAN, *Electromagnetic Scattering on Spherical Polydispersions* , 1969.

L. ELTERMAN , Rayleigh and Extinction Coefficient to 50km for the region 0.27µm to 0.55µm. *Applied Optics,* **10,** 1139-1145, 1964.

SUBROUTINE ODRAYL

Function: To compute the molecular optical depth as a function of wavelength for any atmosphere defined by the pressure and temperature profiles.

Description: The optical depth is written

$$\tau_\lambda^R = \int_0^{+\infty} \beta_\lambda(z)\, dz$$

where $\beta_\lambda(z)$ is the molecular extinction coefficient at altitude z and for wavelength λ. It can be obtained from

$$\beta_\lambda(z) = \sigma_\lambda\ N_r(z) 10^5,$$

with $N_r(z)$ is the molecules number/cm^3 at altitude z, and σ_λ the extinction (or scattering) cross section in cm^2.

These two quantities are defined by

$$\sigma_\lambda = \frac{8\Pi^3 (n_s^2 - 1)^2}{3\lambda^4 N_s^2} \frac{6 + 3\lambda}{6 - 7\lambda}$$

and

$$N_r(z) = N_s \frac{P(z)}{1013.25} \frac{273.15}{T(z)}$$

where P(z) and T(z) are respectively the pressure and the temperature at the altitude z. Recall that n_S is the air refractive index, N_S the molecular density at z=0 in STP conditions, and δ the molecular depolarization factor.

We have taken:

* for refractive index

$$(n_s - 1).10^8 = 8342.13 + \frac{2406030}{130 - \nu^2} + \frac{15997}{38.9 - \nu^2}$$

where ν is the frequency in cm^{-1}

* $N_S = 2.54143.10^{19}$
* and the depolarization factor $\delta = 0.0279$ following *Young*'s (1980).

This depolarization factor is also used to compute the Rayleigh phase function (see routine CHAND.f) according to:

$$P(\Theta) = \frac{3}{4}\frac{1-\gamma}{1+2\gamma}(1+\cos^2\Theta) + \frac{3\gamma}{1+2\gamma}$$

where Θ is the scattering angle, and $\gamma = \delta/(2-\delta)$.

References :

B. EDLEN, The refractive Index of Air. *Meteorologia,* **2,** 71-80, 1966

L. ETERMAN, Rayleigh and Extinction Coefficients to 50 km for the Region 0.27 μm to 0.55 μm *Appl. Opt*., 10, p. 1139-1145, 1964

D.V. HOYT, A redetermination of the Rayleigh Optical Depth and its Application to selected Solar Radiation Problems, *J. Appl. Meteor*, 16, p. 432-436, 1977.

A. T. YOUNG, Revised Depolarization Corrections for Atmospheric Extinction. *Applied Optics,* **19,** 3427-3428, 1980

SUBROUTINE OS

Function: Compute the atmospheric intrinsic reflectance for the case of either satellite or aircraft observation. Also compute the downward radiation field needed by the integral formula of $\bar{\rho}$ and $\bar{\rho}'$ (see Chapter I, §2.5.1, Eqs. 25 and 26) used in the computation in case of a non lambertian target.

Description: The general purpose of the successive order of scattering is to solve numericaly the equation of radiative transfer for upward (Eq. 01.) and downward radiation (Eq. 02.) at any optical thickness τ. If τ_1 is the total optical thickness and μ the cosine of the view angle, then we can write:

$$I(\tau;\mu,\varphi) = I(\tau_1;\mu,\varphi)\, e^{-(\tau_1-\tau)/\mu} + \int_{\tau}^{\tau_1} J(\tau';\mu,\varphi)\, e^{-(\tau'-\tau)/\mu}\, \frac{d\tau'}{\mu} \quad (1 \geq \mu \geq 0) \qquad (01)$$

$$I(\tau;-\mu,\varphi) = I(0;-\mu,\varphi)\, e^{-\tau/\mu} + \int_{0}^{\tau} J(\tau';-\mu,\varphi)\, e^{-(\tau'-\tau)/\mu}\, \frac{d\tau'}{\mu} \quad (1 \geq \mu \geq 0) \qquad (02)$$

where the source function, $J(\tau;\mu,\varphi)$ accounts for the interaction of the present radiation field with the particles of the layer located at τ, so that:

$$J(\tau;\mu,\varphi) = \frac{\omega_0}{4\Pi} \int_{0}^{2\pi} \int_{-1}^{1} I(\tau;\mu',\varphi')\, P(\mu,\varphi;\mu',\varphi')\, d\mu'\, d\varphi' + \frac{\omega_0}{4\pi}\, \pi F_0\, P(\mu,\varphi;-\mu_0,\varphi_0)\, e^{-\tau/\mu_0} \qquad (03)$$

The second term of equation (03) represents the sun source F_0 transversing the path along (μ_0,φ_0) directly to the level τ and then being scattered in direction (μ,φ) (primary scattering).

To solve this differential equation, one has to fix boundary conditions which are:

$$I(0;-\mu,\varphi) = 0 \qquad (04)$$

$$I(\tau_1;\mu,\varphi) = 0 \qquad (05)$$

These express the fact that there is no diffuse downward nor upward radiation at the top and the bottom of the finite atmosphere.

The convention is to describe the atmosphere with the top at $\tau=0$ and the bottom at $\tau=\tau_1$. The upward radiation correspond to $+\mu$ and the downward to $-\mu$ with $(1\geq\mu>0)$ as depicted by figure 1.

Figure 1: Schematic view of the radiative transfer problem for a plane parralel atmosphere.

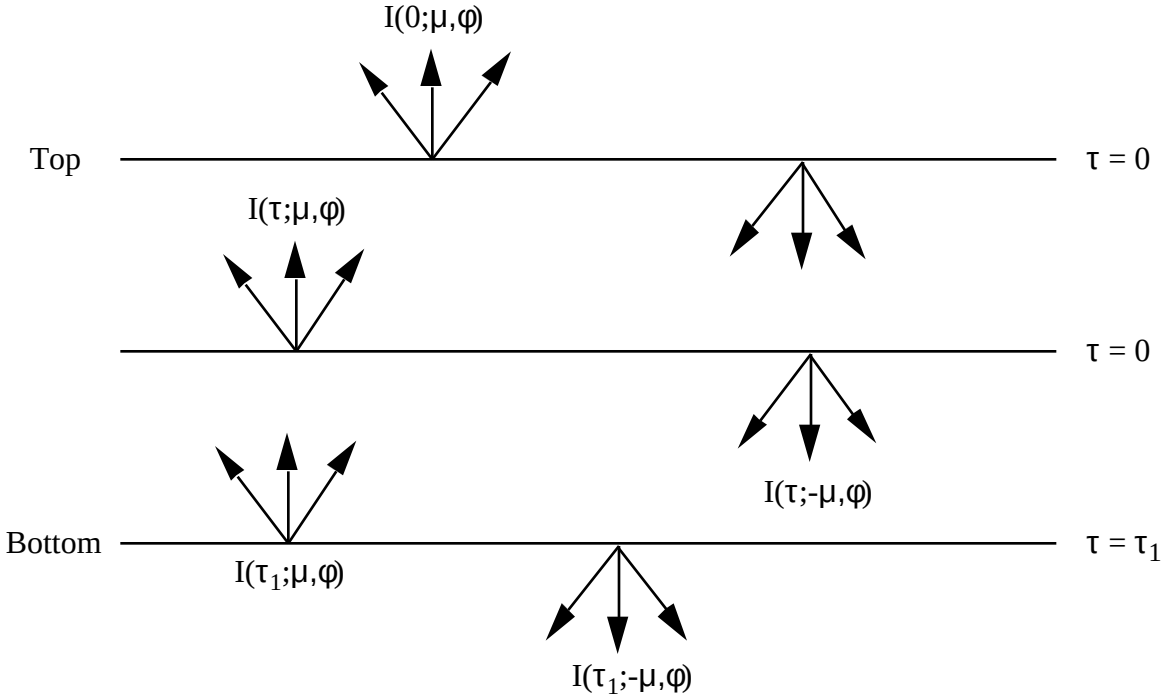

The successive orders of scattering consist of solving numerically the equation of transfer by iteration. First, the equation is solved for each layer considering only the primary scattering radiation (one interaction between the source (sun) and the atmosphere), giving for Eqs. (01) and (02):

$$I^{(1)}(\tau;\mu,\varphi) = \frac{\omega_0}{4\pi}\,\pi F_0\; P(\mu,\varphi;-\mu_0,\varphi_0)\, e^{-\tau/\mu_0} \qquad (1\geq\mu\geq 0) \qquad (06)$$

$$I^{(1)}(\tau;-\mu,\varphi) = \frac{\omega_0}{4\pi}\,\pi F_0\; P(-\mu,\varphi;-\mu_0,\varphi_0)\, e^{-\tau/\mu_0} \qquad (1\geq\mu\geq 0) \qquad (07)$$

Then for higher order of scattering we write:

$$I^{(n)}(\tau_j;\mu,\varphi) = \frac{1}{\mu}\sum_{i=j}^{p} J^{(n)}(\tau_j;\mu,\varphi)\, e^{-\left[(\tau_j-\tau)/\mu\right]}\Delta\tau \qquad (08)$$

$$I^{(n)}(\tau_j;-\mu,\varphi) = \frac{1}{\mu}\sum_{i=1}^{j} J^{(n)}(\tau_j;-\mu,\varphi)\, e^{-\left[(\tau-\tau_j)/\mu\right]}\Delta\tau \qquad (09)$$

where p represents the number of layers used for the decomposition of the atmosphere, τ_j the optical thickness at level j and $\Delta\tau$ the increment in optical thickness between two successive layer. $J^{(n)}$ is computed from $I^{(n-1)}$ by:

$$J^{(n)}(\tau;\mu,\varphi) = \frac{\omega_0}{4\Pi}\int_0^{2\pi}\int_{-1}^{1} I^{(n)}(\tau;\mu',\varphi')P(\mu,\varphi;\mu',\varphi')\,d\mu'\,d\varphi' \qquad (10)$$

In the code a numerical integration of Eq. 10 is performed using the decomposition in Fourier series (for φ), the legendre polynomial and Gaussian quadrature (for μ).

SUBROUTINE SCATRA

Function: To compute the scattering transmission functions for the three atmospheric models, rayleigh, aerosol and a mixture of both on the two paths (downward and upward). We also compute the spherical albedo.

Description: As in ATMREF.f, we have to compute the transmission function and albedo in three different cases and three sensor configurations. Again, the accuracy of the computation of 6S was a concern, so the approximation adopted in 5S has been replaced by using the sucessive order of scattering method (ISO.f) for the aerosol case and the mixed case, or when the sensor was inside the atmosphere on board an aircraft. For the Rayleigh atmosphere we used an accurate analytical formula which has sufficient accuracy and enables us to save computer time. The formula is explicity coded into SCATRA.f for the transmission and call CSALBR.f for the albedo. For ground measurements, the upward transmission is set to 1.0 and the spherical albedo to 0.0, because we neglect the atmosphere between the sensor and the target.

We only give here the formula of the Rayleigh transmission which is based on the two stream method adapted to the case of a single scattering albedo equal to 1.0 (Rayleigh case). The total transmission on path of length μ, T(μ) can be approximated by:

$$T(\mu) = \frac{[(2/3) + \mu] + [(2/3) - \mu] e^{-\frac{\tau^R}{\mu}}}{(4/3) + \tau^R} \qquad (01)$$

where tR is the Rayleigh optical thickness.

Figure 1 compares the accuracy of Eq. 01 to the "exact" computation (Successive Orders of Scattering).

References

J.H. JOSEPH, W.J. WISCOMBE, J.A. WEINMAN, The Delta-Eddington Approximation for Radiative Flux Transfer,.*J. Atmos. Sci*. 33, p.2242-2459, 1976.

W.E. MEADOR, W.R. WEAVER, Two-Stream Approximations to Radiative Transfer in Planetary Atmospheres: a Unified Description of Existing Methods and a New Improvement, *J. Atmos. Sci*. 37, p. 630-643, 1980.

R.H.WELCH, W.G. ZDUNKOWSKI, Back Scattering Approximations and their Influence on Eddington-Type Solar Flux Calculation, *Beitr. Phys. Atmosph.*, 55, no 1, p. 28-42, 1982.

W.G. ZDUNKOWSKI, R.M. WELCH, G. KORB, An Investigation of the Structure of Typical Two-Stream Methods for the Calculation of Solar Fluxes and Heating Rates in Clouds, *Beitr. Phys. Atmosph*.53, no 2, p. 147-166, 1980.

Figure 1: Accuracy of Eq. 01

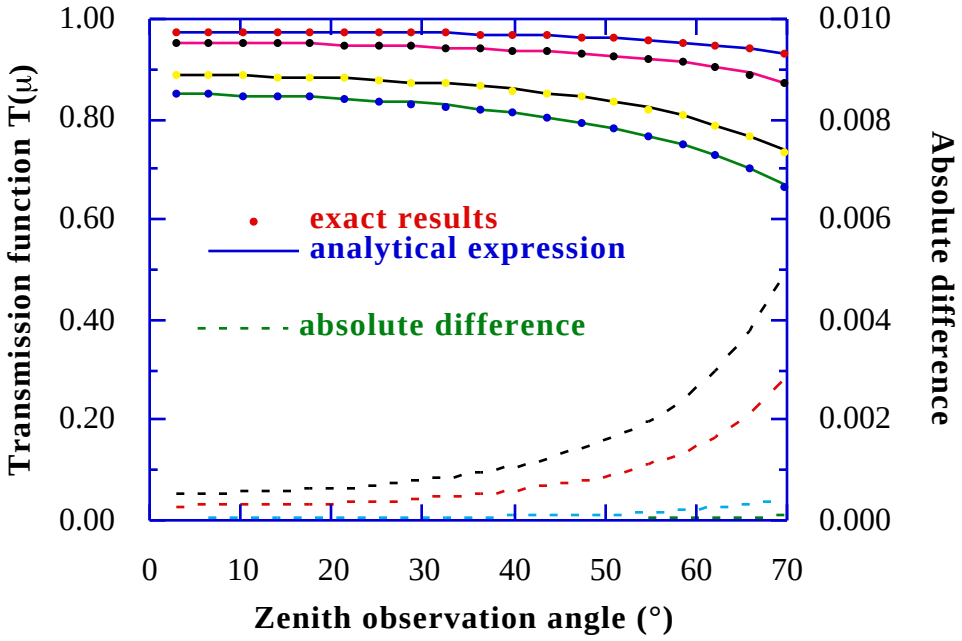

SUBROUTINE TRUNCA

Function: decompose the aerosol phase function in series of Legendre polynomial used in OS.f and ISO.f and compute truncation coefficient f to modify aerosol optical thickness τ and single scattering albedo ω_0 according to:

$$\tau' = (1 - \omega_0 \, f) \, \tau$$

$$\omega_0' = \frac{\omega_0 \, (1 - f)}{(1 - \omega_0 \, f)}$$

References

J. LENOBLE, Radiative Transfer in Scattering and Absorbing Atmospheres: Standard computional procedures, pp 83-84, A. Deepak Publishing, 1985